P-001 HNCA-TOCSY-CANH experiments with alternate ^{13}C-^{12}C labeling: a set of 3D experiment with unique supra-sequential information for mainchain resonance assignment

Koh Takeuchi[1], Maayan Gal[2], Hideo Takahashi[3], Gerhard Wagner[2], and Ichio Shimada[1,4]

[1]Biomedicinal Information Research Center, National Institute of Advanced Industrial Science and Technology, [2]Department of Biochemistry and Molecular Pharmacology, Harvard Medical School, [3]Graduate School of Nanobioscience, Yokohama City University, [4]Graduate School of Pharmacology, The University of Tokyo

ABSTRACT

Described here is a set of three-dimensional (3D) NMR experiments that rely on CACA-TOCSY magnetization transfer via the weak $^{3}J_{C\alpha C\alpha}$ coupling. These pulse sequences, which resemble recently described ^{13}C detected CACA-TOCSY experiments, and use ^{1}H excitation and detection. These experiments require alternate ^{13}C-^{12}C labeling together with perdeuteration, which allows utilizing the small $^{3}J_{C\alpha C\alpha}$ scalar coupling that is otherwise masked by the stronger $^{1}J_{CC}$ couplings in uniformly ^{13}C labeled samples. These new experiments provide a unique assignment ladder-mark that yields bidirectional supra-sequential information and can readily straddle proline residues.

INTRODUCTION

Establishing sequence-specific assignments is fundamental for structural analysis of biological macromolecules using NMR spectroscopy. Numerous pulse sequences have been developed to assign resonances to the right nuclei in the polypeptide sequence. The foremost basic experiments for protein backbone assignment, such as the HNCA and HNcoCA, correlate a ^{15}N-^{1}H spin pair to the preceding $^{13}C^{\alpha}_{i-1}$. Where coincidental overlap of C^{α} signals prevents unambiguous assignments, experiments correlating sidechain resonances can be recorded. Typically, these experiments rely on matching the carbon frequencies measured in the set of 3D experiments. However, often severe cases of overlap still exist, which increases the chance of incorrect assignments. In cases where carbon signals overlap, especially for Gly, which lacks C^{β}, relying on the better dispersed ^{15}N can be advantageous. This can be done with a set of pulse sequences that correlate a pair of ^{15}N-^{1}H nuclei directly to the adjacent N and/or H (*i-1* and *i+1*) in a single experiment, such as the HNcocaNH and HNcaNH. These experiments are valuable when dealing with large molecular weight or unstructured proteins.

Although the basic set of triple resonance experiments proofed to be robust, the exclusive use of ^{13}C-^{15}N and ^{15}N-^{1}H direct scalar coupling for INEPT-based coherence transfer limits the number of sequential correlations that can be observed in these types of experiments. Indeed, detecting a correlation that couples an ^{15}N-^{1}H spin pair with the succeeding $^{13}C^{\alpha}_{i+1}$, or nuclei separated by more than one residue is not straight forward due to the absence of strong scalar coupling connecting these nuclei. However, obtaining these longer-range through-bond correlations

Mainchain resonance assignment, CACA-TOCSY, Alternate ^{13}C-^{12}C labeling

is potentially very useful for preventing incorrect assignments due to accidental peak degeneracy.

Very recently, we have shown that utilizing TOCSY in ^{13}C detected experiments together with alternate ^{13}C-^{12}C labeling (CACA-TOCSY), enables direct connections between $^{13}C^{\alpha}$ nuclei in adjacent amino acids via the weak long-range ^{3}J coupling (~2 Hz)[1]. In uniformly ^{13}C labeled samples, these weak couplings are masked by the strong ^{1}J carbon-carbon splitting but are readily observed in proteins expressed with the alternate ^{13}C-^{12}C labeling scheme. Since the heteronuclear ^{13}C-^{15}N scalar couplings are preserved in the labeling scheme, the CACA-TOCSY experiment can easily be integrated into the conventional NH-detected set of 3D experiments.

Here we describe a set of proton-detected 3D NMR experiments utilizing the long-range $^{3}J_{C\alpha C\alpha}$ coupling, namely the hnCA-TOCSY-caNH, hNca-TOCSY-caNH, and Hnca-TOCSY-caNH (Figure 1)[2]. All of these experiments share the same coherence pathways and the ability to provide unique bidirectional supra-sequential correlations. The merits of the experiments are two-fold. (1) This set of experiments can be used without or in addition to the conventional 3D experiments to avoid the previously described degeneracy problems, as simultaneous observation of more than two sequential correlation peaks makes assignment easier and more reliable. (2) The assignment procedure can also bridge breaks in sequential connectivity introduced by single proline (Pro) residues. As the Pro residues lack the amide proton, the correlation originating from this residue cannot be detected in a conventional 3D experiments. However, the supra-sequential correlation obtained here can bypass these gaps by directly connecting residues preceding and succeeding prolines.

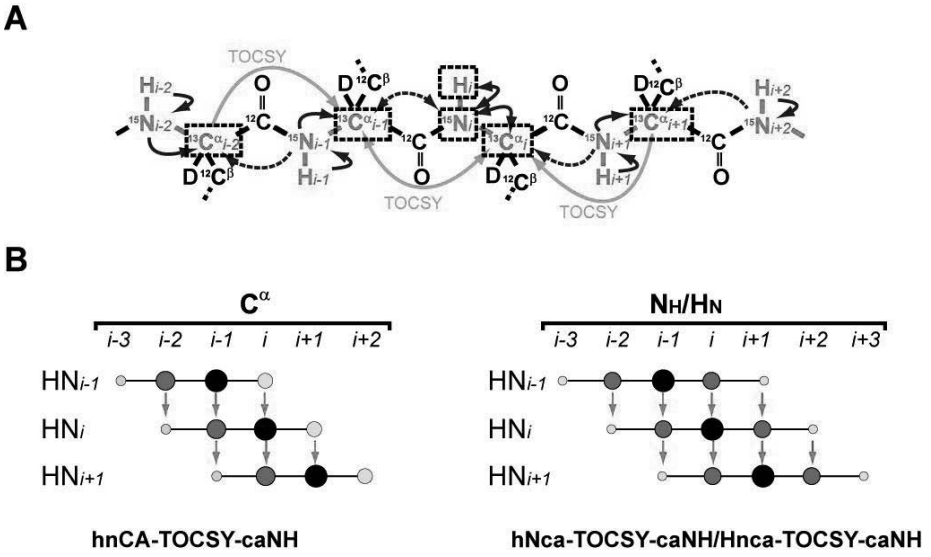

Figure 1. Experimental design for the 3D experiments utilizing the CA-CA TOCSY transfer. (A) Illustration of the coherences utilized in the 3D hnCA-TOCSY-caNH experiment. The nuclei involved in this experiment are colored in red. Arrows indicate the coherence transfer pathways in the hnCA-TOCSY-caNH experiment, which are eventually detected as HN_i. Blue solid and dotted arrows indicate coherence transfers via $^{1}J_{NC\alpha}$ and $^{2}J_{NC\alpha}$ heteronuclear scalar couplings. On the other hand, yellow arrows indicate coherence transfers via $^{3}J_{C\alpha C\alpha}$ TOCSY. The nuclei that are correlated to HN_i are boxed with black broken lines. (B) Schematic representation of the observed coherences in the 3D hnCA-TOCSY-caNH experiment. Larger and darker peak sizes indicate higher intensities.

RESULTS and DISCUSSION

Figure 1A shows the coherence transfer pathway in the 3D hnCA-TOCSY-caNH NMR experiment. The pulse sequence correlates each ^{15}N-^{1}H pair of residue *i* to the sequentially adjacent C$^{\alpha}$s at positions *i-2* to *i+1*, as shown in Figure 1B. Unlike the conventional HNCA and HNcoCA experiments, which only provide a sequential ^{13}C$^{\alpha}$ correlation to the preceding residue, the 3D hnCA-TOCSY-caNH experiment provides sequential connectivity for ^{13}C$^{\alpha}$s in both directions. Clearly, this unique feature yields more reliable assignments in case that the preceding ^{13}C$^{\alpha}$ resonance of a certain residue *i* is degenerate with the ^{13}C$^{\alpha}$ of a different residue.

To test this new experimental scheme we have recorded the 3D hnCA-TOCSY-caNH experiment on uniformly ^{2}H^{15}N and alternately ^{13}C-^{12}C labeled B1 domain of protein G (GB1) produced with 2-^{13}C glycerol as the only carbon source to maximize the ^{13}C$^{\alpha}$ labeling rate[3]. The protein was dissolved in H_2O-based buffer, and the data were recorded on a 600 MHz magnet, equipped with a cryogenic probe. To simulate correlation times of a 40 kDa protein, 40% glycerol was added to the buffer while the temperature was kept at 298 K. The rotational correlation time estimated by the [^{15}N, ^{1}H]-TRACT experiment was 18 ns at this condition. In order to transfer magnetization between different C$^{\alpha}$s by isotropic mixing, a duration of 132-ms was experimentally calibrated for optimal transfer.

Figure 2A shows ω1 (^{13}C$^{\alpha}$) / ω3 (^{1}H^{N}) strips from the 3D hnCA-TOCSY-caNH spectrum of GB1 with the above experimental settings. For demonstration, only strips showing the sequential connectivity of residues Thr49 to Thr53 are depicted. As shown in the figure, both $^{13}C_{i-1}$ and $^{13}C_{i+1}$ correlations are observed. These bidirectional correlations are essential in avoiding degeneracy in the preceding C$^{\alpha}$ correlation ($^{13}C_{i-1}$). This is clearly exemplified in Figure 2B. When trying to determine the strip originating from Thr44 based on the $^{13}C_{i-1}$ signal in the Tyr45 strip (signal at 57.4 ppm), the HNCA spectrum provides three different candidates (#1~3). However, if the additional data from the hnCA-TOCSY-caNH experiment are used, one can unambiguously identify strip #1 as representing the correlations to Thr44 by checking the strip that contains the correlation to the ^{13}C$^{\alpha}$ signal of Tyr45. The experiment also provides a unique connectivity between the ^{15}N-^{1}H pair of residue *i* to the C$^{\alpha}$ at positions *i-2*. Since the transfer pathway from the $^{15}N_i$-$^{1}H_i$ spin pair to C^{α}_{i-2} does not involve the amide moiety of residue *i-1*, the correlation can be observed even if the residue *i-1* is a proline. This suggests that the experiment can skip single Pro residue gaps, which usually cause breaks in sequential assignments in conventional HNCA type of experiments. Without any exception, all of the ^{15}N-^{1}H pairs had correlations to $^{13}C^{\alpha}_{i}$ and $^{13}C^{\alpha}_{i-1}$. In addition, 44 residues (81 %) have a bidirectional sequential correlation to the $^{13}C^{\alpha}_{i+1}$. The missing resonances are those involving residues with less than 20% ^{13}C$^{\alpha}$ labeling rate. In addition, valuable supra-sequential correlations for $^{13}C^{\alpha}_{i-2}$ were observed for a significant number of residues (23/53 residues, 43%).

The hnCA-TOCSY-caNH experiment can also be combined with a different type of chemical shift encoding. For example, in the hNca-TOCSY-caNH experiment, a nitrogen evolution is used instead of the ^{13}C$^{\alpha}$ *t1* evolution. For the Hnca-TOCSY-caNH experiment, a proton evolution was used for *t1* evolution. In these spectra, a ^{15}N-^{1}H pair of residue *i* is directly coupled to the adjacent H^{N} or N^{H} at positions *i-2* ~ *i+2*, respectively (Figure 1B, right). In the hNca-TOCSY-caNH experiment, 50/54 (92 %) and 47/54 (87 %) of ^{15}N-^{1}H pairs have correlations to N_{i-1} and N_{i+1}, respectively. As for Supra-sequential correlations, 20/53(38 %) of N_{i-2}, and 13/53 (25 %) of N_{i+2} correlations were observed. Although bidirectional sequential connectivities obtained from these

experiments are useful to resolve resonance overlap, the information does not contain the direction in the amino acid sequence. Thus, complementary use with unidirectional experiment such as hNcocaNH and HncocaNH would be beneficial.

In addition to the concentrated GB1 standard sample, we have tested the pulse sequence on the low concentrated (150 μM) 17kDa unfolded regulatory domain of nuclear factor of activated T cells (NFAT) that contains many phosphorylation sites and pralines. The results on the protein would be provided in the poster.

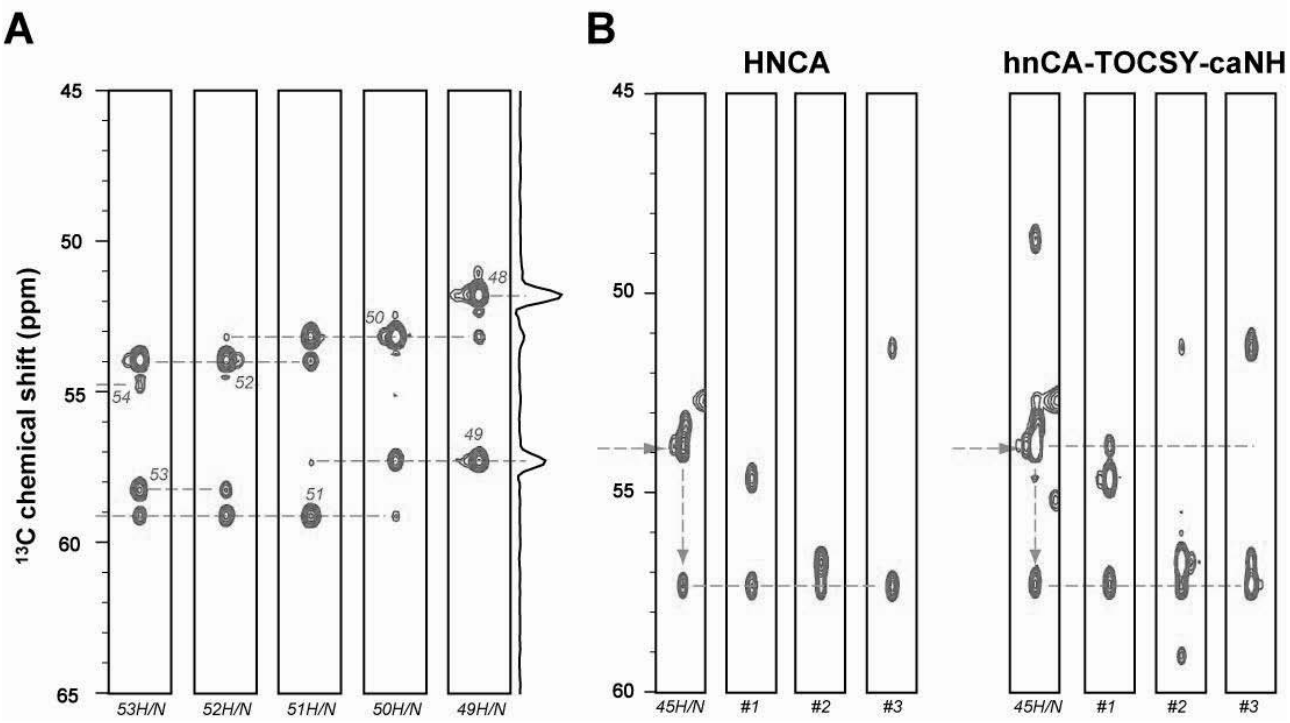

Figure 2. Sequential backbone assignments with the 3D hnCA-TOCSY-caNH experiment. (A) Representative ω_1 ($^{13}C^{\alpha}$) / ω_3 ($^{1}H_N$) strips from the 3D hnCA-TOCSY-caNH spectrum of GB1 connecting Thr49 to Thr53. The experiment was recorded on a Bruker AVANCE 600 spectrometer equipped with a cryogenic probe, using a 3.5 mM sample of the uniformly $^{2}H^{15}N$ and alternately ^{13}C-^{12}C labeled B1 domain of protein G (GB1) in H_2O. Sequential correlation peaks are shown by broken lines. For each increment, 16 scans were acquired. (B) Assignment procedure by the complementary use of HNCA and hnCA-TOCSY-caNH experiments. The HNCA ω_1 ($^{13}C^{\alpha}$) / ω_3 ($^{1}H_N$) strips at the ^{15}N position of Tyr45 are shown in the left panel. The horizontal arrow indicates the chemical shift of Tyr45 $^{13}C^{\alpha}$, whereas the vertical arrow connects Tyr45 $^{13}C^{\alpha}$ to Thr44 $^{13}C^{\alpha}$.

1. Takeuchi K., Frueh D, Sun Z, Hiller S, and Wagner G (2010) CACA-TOCSY with alternate ^{13}C-^{12}C labeling: a $^{13}C^{\alpha}$ direct detection experiment for mainchain resonance assignment, dihedral angle information, and amino acid type identification. *J Biomol NMR*, 47, 55-63
2. Takeuchi K, Gal M, Takahashi H, Shimada I, and Wagner G (2011) HNCA-TOCSY-CANH experiments with alternate ^{13}C-^{12}C labeling: a set of 3D experiment with unique supra-sequential information for mainchain resonance assignment. *J Biomol NMR*, 49, 17-26
3. Takeuchi K, Sun ZY, and Wagner G (2008) Alternate ^{13}C-^{12}C labeling for complete mainchain resonance assignments using C^{α} direct-detection with applicability toward fast relaxing protein systems. *J Am Chem Soc*, 130, 17210-17211

P-002 Capillaries Can Prevent Thermal Convection in an NMR Tube

Takashi Iwashita, Tsuyoshi Konuma and Kenji Sugase
NMR Group, Division of Organic Chemistry, Suntory Foundation for Life Sciences, Bioorganic Research Institute

The DOSY (Diffusion Ordered SpectroscopY) is very sensitive to thermal convection, which is caused easily by a low air flow in a probe head. The smaller diameter sample tubes and the sample tube spinning have been proposed to prevent the thermal convection. We found that capillaries can be used for the same purpose. In our method, fifteen to eighteen 0.8-mm diameter capillaries are inserted in a 5-mm diameter regular NMR tube. The capillaries can effectively prevent the thermal convection, enabling us to obtain clean DOSY spectra.

[Introduction] The DOSY (Diffusion Ordered SpectroscopY)[1], a method to determine translational diffusion constants, is very sensitive to thermal convection, which is caused easily by a low air flow in a probe head. If there is thermal convection in an NMR tube on DOSY experiments, the spectra shows many fake peaks, and thus it is difficult to obtain the true diffusion rate. The air flow rate is one of important factors of thermal convection, and should not be used at the low level. Additionally, various methods have been proposed to prevent thermal convection. For example, the use of a small outer diameter (OD) sample tube and/or sample tube spinning was recommended to prevent thermal convection.[2] However, the sample volume of a 3-mm OD tube is one-third of a 5-mm OD tube, so that the S/N ratios using a 3-mm OD tube are lower than those using a 5-mm OD tube, resulting in the lower spectra quality. The sample tube spinning is an easy way, and a 5-mm OD regular NMR tube can be used. However, it brings down side-effects like spinning side band.

In this study, we looked for an easy method to prevent thermal convection using a regular 5-mm OD sample tube, and found that capillary insertion efficiently prevents thermal convection. The inserted capillaries make small compartments in the NMR tube, and the solution does not flow across these small compartments. This small-compartment effect makes prevention of thermal convection, and the solution components would move according to natural diffusion phenomena.

[Experimental] The DOSY experiments were performed on a mixture of Cinchonidine (**1**:MW 294.40) and *m*-Cresol (**2**:MW 180.14) using AVANCE-750 spectrometer (Bruker, ^{1}H:750 MHz) with a CryoProbe TCI-Z. The air flow rate was 670 L/h, and the probe temperature was 25 degrees Celsius. Fifteen to eighteen 0.8-mm diameter capillaries (Nippon Electric Glass Co., Ltd.) were inserted into a regular 5-mm OD NMR tube, and were longitudinally aligned in the NMR tube. The 0.8-mm OD capillary has 0.4-mm inner diameter (ID), so that the glass part of eighteen capillaries occupy a half of inner area of a regular 5-mm OD NMR tube. The 300 µl of solution was placed in a regular 5-mm OD NMR tube in consideration of the capillarity effect. Tuning of the magnetic field homogeneity was performed by a standard gradient shimming routine for Z-axis, and the resulting line shape was almost identical to that using a regular 5-mm OD NMR tube.

Thermal Convection, DOSY, Capillaries

[Results and Discussion] Figure 1 shows appearances of a capillary and a regular 5-mm OD NMR tube containing eighteen capillaries and the sample solution. The 300 μl of solution had enough height for the NMR coil.

In the case of a regular NMR tube, the DOSY spectrum of a mixture of Cinchonidine (**1**) and *m*-Cresol (**2**) in $CDCl_3$ had fake peaks in Figure 2 A), even with the air flow rate of 670 L/h. However, when fifteen 0.8-mm OD capillaries were inserted into a regular 5-mm OD NMR tube, the components Cinchonidine (**1**) and *m*-Cresol (**2**) were separated clearly by their diffusion rate as shown in Figure 2 B).

The capillaries can prevent thermal convection effectively without any special tools. It can be applied on all of the samples that would be influenced by thermal convection. The longitudinally aligned capillaries had no bad effects for the component of Z-axis magnetic field homogeneity. It ensures the high quality of spectra.

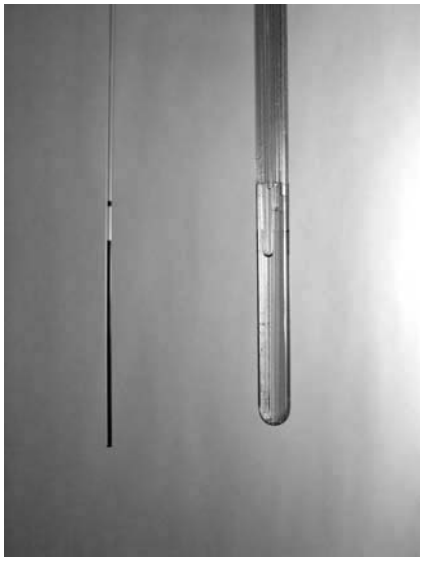

Figure 1. Capillary and NMR tube

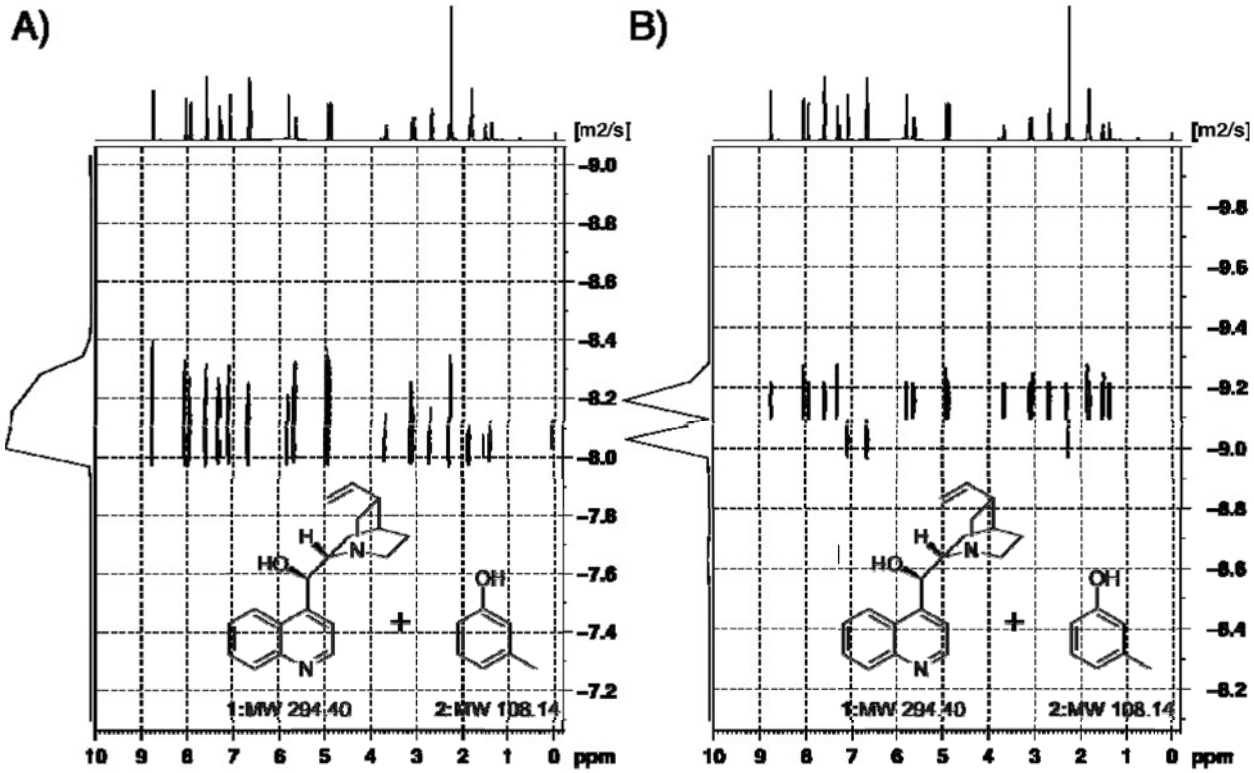

Figure 2. The DOSY spectra of a mixture of Cinchonidine (**1**) and *m*-Cresol (**2**) in $CDCl_3$.
A):Standard 5-mm OD NMR tube, B):Fifteen 0.8-mm OD capillaries were inserted in a standard 5-mm OD NMR tube.

[References]

1) D. Wu, A. Chen and C. S. Johnson Jr., *J. Magn. Reson.*, **A115**, 260-264 (1995)
2) N. Esturau, F. Sánchez-Ferrando, J. A. Gavin, C. Roumestand, M.-A. Delsuc and T. Parella, *J. Magn. Reson.*, **153**, 48-55 (2001)

P-003 Convenient method for modulating the direction of the magnetic susceptibility tensor relative to the target protein and its application for PCS-based protein-protein complex structure determination

Yoshihiro Kobashigawa[1], Tomohide Saio[1], Masahiro Ushio[2], Mitsuhiro Sekiguchi[3], Masashi Yokochi[1], Kenji Ogura[1], Fuyuhiko Inagaki[1]

[1]Department of Structural Biology, Faculty of Advanced Life Science, Hokkaido University.

[2]Graduate School of Life Science, Hokkaido University.

[3]Analysis and Pharmacokinetics Research Labs. Department of Drug Discovery, Astellas Pharma Inc.

[**ABSTRACT**]

Pseudo contact shifts (PCSs) induced by paramagnetic lanthanide ions fixed in a protein frame provide long-range distance and angular information, and are valuable for structure determination of protein-protein complexes. However, PCS-based rigid body docking studies exhibit degenerate solutions due to symmetry of the magnetic susceptibility tensor. Though the use of another PCS data set derived from the lanthanide ion fixed at a different position can resolve this degeneracy, it is not straightforward to find several tagging points. Here we presented a convenient method to modulate the direction of the magnetic susceptibility tensor relative to the target protein, and demonstrated that this approach was useful and practical for resolving the degeneracy problem.

Key words: docking, lanthanide, protein complex

Long-range distance and angular information is useful for the structural analysis of large proteins, multidomain proteins and protein complexes. Paramagnetic lanthanide ions induce several NMR effects on observed nuclei, including a pseudo-contact shift (PCS) and a residual dipolar coupling (RDC), due to anisotropy of the magnetic susceptibility tensor ($\Delta\chi$-tensor). The PCS provides distance and angular information between the lanthanide ion and the observed nuclei situated up to approximately 40 Å from the lanthanide ion, whereas the RDC provides molecular

alignment information independent of distance. Therefore, the paramagnetic lanthanide ions are useful probes for structure determination by NMR. For application of the paramagnetic lanthanide probe to non-metalloproteins, we developed two-point anchored lanthanide binding peptide tag (LBT: CYVDTNNDGAYEGDEL)[1-4], where LBT was linked to the target protein via two anchoring points, a disulfide bridge and an N-terminal fusion[5]. The two-point anchored LBT has advantage in availability for protein NMR researchers, since it can be expressed as a fusion protein with the target protein using *E.coli* and presumably other hosts. This method was first applied to the B1 immunoglobulin binding domain of protein G (GB1) as a model protein to evaluate the $\Delta\chi$-tensor of the paramagnetic lanthanide ion[5]. Then we applied TALAP to a PCS-based structure determination of a protein-protein complex[6], drug screening, and structure determination of a drug-protein complex[7]. However, magnetic susceptibility tensor has a symmetry (Fig. 1), which gives eight degenerate solutions in a structure determination based only on PCS restraints. The degeneracy cannot be fully resolved by combined use of multiple PCS data sets from several lanthanide ions fixed using a common tagging system[6] (Fig. 2). In order to overcome this degeneracy, it is crucial to obtain another PCS data set that possesses different directions of of the principal axes and a different position of the paramagnetic center relative to the target protein. Several sets of the data are available by introducing the tag at different positions on the target

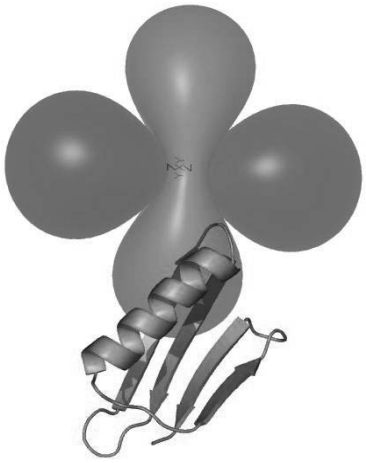

Fig.1: Symmetry of PCS-isosurface[5].

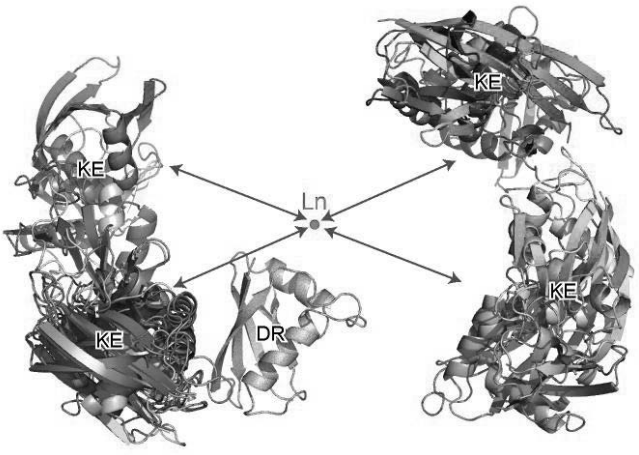

Fig.2. Degeneracy of the protein-protein complex structure obtained based only on PCS [6].

protein. In many cases, however, it is not straightforward to find several fixing point for tagging.

Here we show that the direction of the principal axes of the Δχ-tensor and the metal position relative to the target proteins can be conveniently modulated by the modification of the spacer length between LBT and the target protein (Fig. 3). This was first confirmed for FKBP12 (Fig. 4), and further for other protein systems, GB1 and Grb2 SH2 domain. We found that tensor axis was changed about 30° for FKBP12 and GB1, about 20° for Grb2 SH2 domain only by changing spacer length of 1 A.A. residue. Moreover, we applied this approach for determination of the rigid body docking structure between FKBP12-rapamycin and mTOR FRB domain based only on PCS restraints, and demonstrated that degeneracy could be resolved by using PCS data sets obtained from two different spacer length LBT-attached constructs (Fig. 5). Present study will markedly increase the usefulness of TALAP system for protein complex structure determination.

We will also present fast and systematic method to design the spacer length and anchoring point for structural analysis using the two-point anchored LBT attached protein.

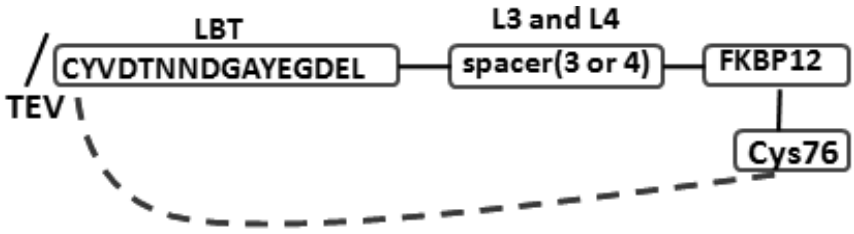

Fig.3. Schematic representation of TALAP attached FKBP12 with 3 (L3) and 4 (L4) amino acid length spacer between LBT and FKBP12.

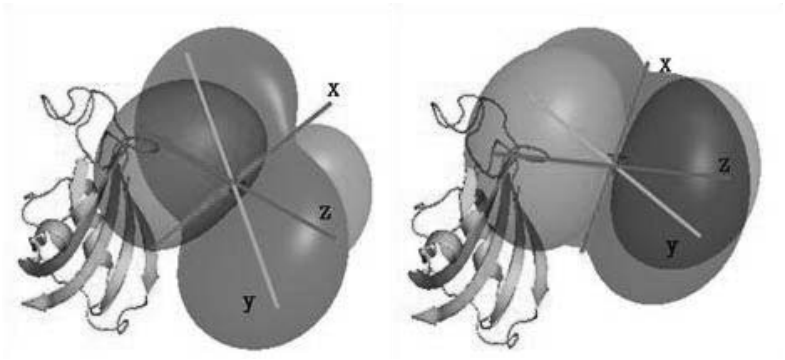

Fig.4. PCS-isosurface of L3 (left) and L4 (right)-FKBP12.

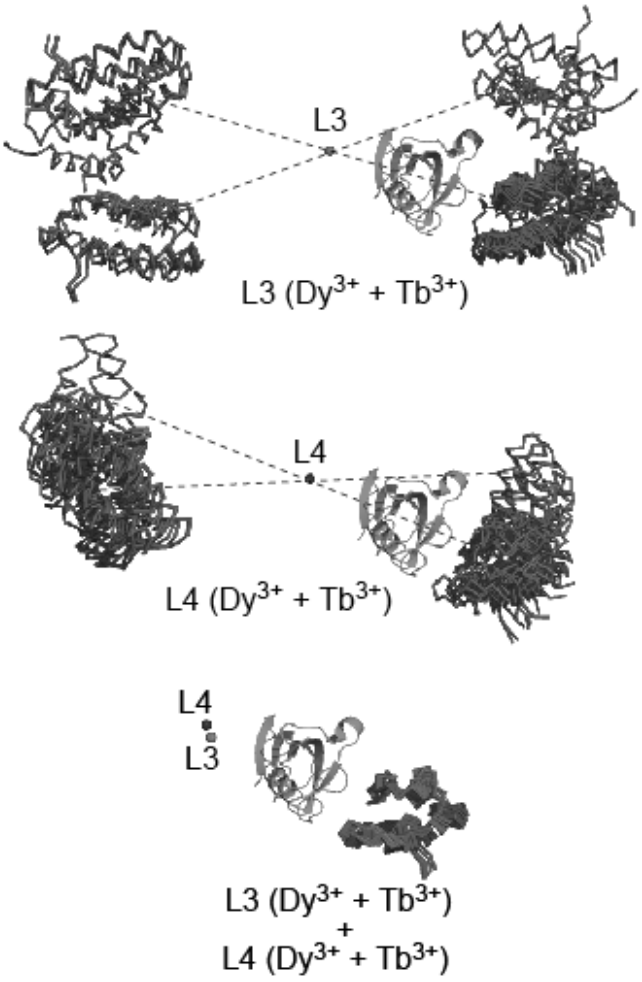

Fig.5. Docking structure between FKBP12 and mTOR FRB domain based only on PCS obtained from L3-FKBP12 (upper panel), L4-FKBP12 (middle panel) and both L3- and L4-FKBP12 (lower panel). FKBP12 is shown in ribbon, and mTOR FRB in Cα-trace. Red (L3) and blue (L4) sphere represents metal position.

[REFERENCES]

(1) Nitz M. *et al*., (2003) *Chembiochem* **4**:272–276.

(2) Nitz M. *et al*., (2004) *Angew Chem Int Ed Engl* **12**:3682–3685.

(3) Su XC. *et al*., (2006) *ChemBioChem* **7**:1599–1604.

(4) Su XC. *et al*., (2008) *J Am Chem Soc* 130:1681–1687.

(5) Saio T. *et al*., (2009) *J Biomol NMR* **44**:157–166.

(6) Saio T. *et al*., (2010) *J Biomol NMR* 46:271-280.

(7) Saio T. *et al*., (2011) *J Biomol NMR in press*

P-004 Signal assignment approaches for ^{13}C labeled lignocellulose by multidimensional NMR spectroscopy

Takanori Komatsu[1], Keiko Okushita[1], Jun Kikuchi[1,2,3,4]
[1]Grad. Sch. BionanoSci., Yokohama City Univ., Japan; [2]RIKEN Plant Science Center, Japan; [3]RIKEN Biomass Eng. Prg., Japan; and [4]Grad. Sch. Bioagri., Nagoya Univ.

ABSTRACT

Signal assignment by NMR spectroscopy contributes analyzing composition and higher-order structure of lignocellulose, however it is hampered by peak overlaps and difficulties of separation and refinement of components. In this study, we propose the approach for signal assignment of lignocellulose by overcoming peak overlaps using 2D (*e.g.*, HSQC, HMBC, HSQC-TOCSY, INADEQUATE, LASSY), and 3D NMR methods (*e.g.*, TOCSY-HSQC, HCCH-COSY) observed for highly ^{13}C labelled lignocellulose.

INTRODUCTION

Lignocellulose, major component of plant cell wall, is one of the most abundant and available biomass materials, and the attention toward it is increasing in term of "biorefinery". However, effective uses of lignocellulose are hampered by the complexity of lignocellulose which consist of cellulose microfibrils embedded in a matrix of hemicellulose and pectin with lignin[1)]. So establishing robust, correct, and detailed methods for lignocellulose characterization is expected.

NMR is one of the most suitable methods to reveal structural characters of lignocellulose. In recent years, structural characterizations of lignocellulose are performed by signal assignments on homonuclear and heteronuclear 2D NMR spectroscopy, especially ^{1}H-^{13}C HSQC[2)]. However, signal assignments of lignocellulose by 2D NMR spectra are complicated by overlapped peaks especially in polysaccharide region because of similarities of their chemical structures. In addition, it is preferred to assign signals without separation of components, because separation and refinement of components from lignocellulose are difficult.

^{13}C labelling of lignocellulose allows several applications in NMR because it causes the emergence of transferring ^{13}C-^{13}C magnetization. 3D HCCH-COSY, which needs transferring ^{13}C-^{13}C magnetization in several steps via J couplings, is powerful technique for assignment of lignocellulose because it makes signals more spread. ^{13}C-^{13}C correlation spectroscopy; 2D INADEQUATE and LASSY[3)] (**L**ow **A**bundance **S**ignal transition correlation **S**pectroscop**Y**), is efficient techniques for assignment of ^{13}C-^{13}C skeletons. In this study, we assigned lignocellulose by use of multidimensional NMR spectra of ^{13}C labeled lignocellulose.

EXPELIMENTS

50 mg of ^{13}C labelled corn lignocellulose was ball-milled for 6 hour. Subsequently the ball-milled powder were dissolved by 0.6 ml in deuterated DMSO/Pyridine mixture at 323 K, 0.5 hour and after centrifugation, it was used as a NMR sample. The 2D (*e.g.*, LASSY, INADEQUATE, HSQC, HSQC-TOCSY, HSQC-NOESY, and HMBC) and 3D NMR experiments (*e.g.*, TOCSY-HSQC, NOESY-HSQC and HCCH-COSY) were employed using 700 MHz and 500 MHz NMR spectrometers.

lignocellulose, multidimensional NMR, signal assignment

RESULTS AND DISCUSSION

For signal assignment of polysaccharides, it is efficient to assign C1 signals at first step, because their signals are more spread than C2-C6 signals. **Fig. 1** shows the method to assign C2 signals from C1 signals on LASSY and 2D HSQC-TOCSY spectra. ^{13}C-^{13}C correlations of C1 and C2 residue of polysaccharides were displayed in LASSY, subsequent ^{1}H chemical shifts were given in 2D TOCSY-HSQC. So, it is possible to assign C2 signals from C1 signals easily.

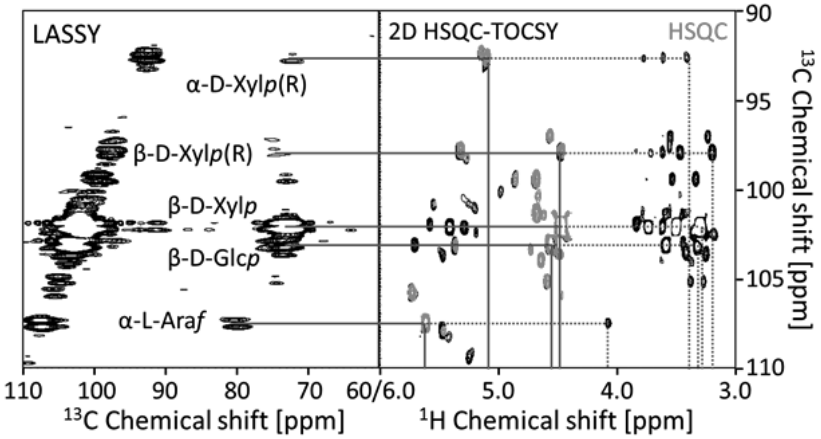

Fig. 1 The method to assign C2 signals from C1 signals on LASSY and 2D HSQC-TOCSY spectra. Solid line shows ^{1}H frequency assignment of C1 residues and dotted line shows that of C2 residue. (R) means reducing end.

Fig. 2 illustrates how 3D TOCSY-HSQC can be effectively used to assign lignocellulose. ^{1}H-^{1}H correlations for neighbouring spins were displayed in each ^{1}H-^{1}H planes, along ^{13}C axis as the third dimension. Therefore, it is possible to assign sequentially each carbon resonance of polysaccharides residue as shown in solid line of **Fig. 2(b)**. Signal separation by ^{13}C axis makes assignment of signals of C2, C3, and C4 residues more easily.

INADEQUATE spectrum of lignocellulose is shown in **Fig. 3**. In the spectrum, two direct bonded carbons share a common double quantum frequency, and along a vertical direction corresponding to a given carbon's single quantum frequency. It is, therefore, possible to assign residue specifically each carbon resonance of polysaccharides. As a results, resonances of β-D-Xyl*p* (X), β-D-Glc*p* (G), and α-L-Ara*f* (A) residue were completely assigned. X2, X3, X5, G2, and G4 signals were overlapped, however they could be separated in the 3D TOCSY-HSQC spectrum. We demonstrated efficient signal assignment was carried out by use of the combination multidimensional NMR included 3D NMR.

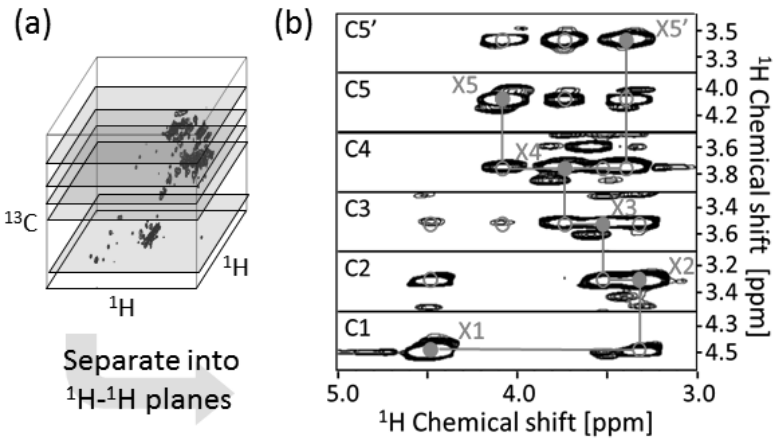

Fig. 2 Assignment approach using 3D TOCSY-HSQC. (a) cubic view of 3D TOCSY-HSQC spectrum. (b) ^{1}H–^{1}H planes at ^{13}C chemical shifts of β-D-Xyl*p* of C5',C5-C1

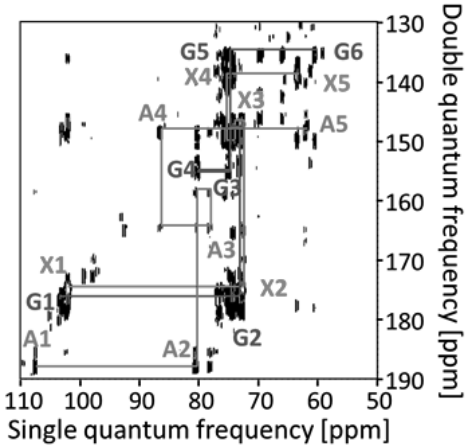

Fig. 3 Residue specific signal assignments of polysaccharides on INADEQUATE spectrum.

References

1) Sarkar, P.; Bosneaga, E.; and Auer, M., *J. Exp. Bot.* **60** (2009) pp. 3615-3635.

2) Kim, H. And Ralph, J., *Org. Biomol. Chem.* **8** (2010) pp. 576-591.

3) Ramesh, V.; George; C.; and Chandrakumar, N., *Chem. Phys. Lett.* **474** (2009) pp. 375-380.

P-006 Y

Tissue-specific biomass profiling of bioenergy plant, *Jastropha curcas.*

Taiji Watanabe[1], Amiu Shino[2], Kinya Akashi [3]and Jun Kikuchi[1,2,4,5]
[1]Grad. Sch. BionanoSci., Yokohama City Univ., Japan; [2]RIKEN Plant Science Center, Japan; [3]Grad. Sch. BiolSci., NAIST, Japan; [4]RIKEN Biomass Eng. Prg., Japan; [5]Grad. Sch. Bioagri., Nagoya Univ.

Abstract.

Jatropha curcas L. has been focus of numerous research due to it`s potential for a new energy source from seed oil. The residual tissues such as stem, seed cake, etc. are also an interesting source of biomass, expected to be used as fertilizer, animal feed and so on. In this research we analyzed different tissues from the plant: stem, bark (bark and phloem), xylem, pith, seed coat, kernel and leaf. Samples were ball-milled, and then dissolved in DMSO-d_6/pyridine-d_5 (4:1) and analyzed in NMR using methods such as 2D HSQC, 2D HSQC-TOCSY and 2D HSQC-NOESY. The signal assignments in HSQC were made according to past researches, and further confirmed by TOCSY and NOESY correlations. Each tissue showed different patterns of lignocellulose composition, *eg.* levels of acetylation in polysaccharides were also different seed coat and xylem showed the highest levels.

1. Introduction.

The current focus of *Jatropha curcas L.* is mainly because of its production of oil from their seeds, but the biomass from the residual tissues produces many other potentially useful products. The residue of the seed can be used for animal feed and biochar, the fibers, for constructions, fertilizer, the seed shell is rich in lignin and may be used for energy generation[1,2,3].

This biomass is mainly originated from the plant cell wall, it is predominantly composed of polysaccharides cellulose, hemicellulose and lignin, these three composing lignocellulose. Cellulose is a β-1,4-linked glucose molecule and all hemicellulosic polysaccharides contain a β-linked sugar backbone. In xylans, mannans, and xyloglucans, the backbone sugars are β-1,4-D-xylose, β-1,4-D-mannose, and β-1,4-D-glucose, respectively, while in glucomannan, the backbone consists of randomly dispersed β-1,4-glucose and β-1,4-mannose sugars. The backbones of hemicellulosic polysaccharides are decorated with a variety of sugars and acetyl groups[4]. Lignin is composed guaiacyl (G), syringyl (S) and *p*-hydroxybenzoates (H) of monolignols and cinnamyl alcohol end group (X1). This monolignols coupling can formed the following substructures: β-O-4 (A), β-5 (B), β-β (C), 5-5/4-O-β (D), 5-O-4 (E) and β-1(F)[5] .

For analysis of lignocellulose NMR techniques are wildly used, 2D NMR-HSQC correlation technique allow direct detection mainly of substructures as A, B, C, D and F besides the monolignols and polysaccharides providing a more specific research of lignocellulose. However the assignments of the peaks are still not complete[6]. Biomass products when employed in energy generation or biochar, in some situations, pretreatments are essential. One of the techniques applied is torrefaction, it is a thermal pretreatment where the biomass is heated in temperatures between 200℃ to 300 ℃[7].

In this research we object to increase assignment data of 2D NMR-HSQC, characterize the different tissue of *Jatropha curcas* and analyze the effects of torrefaction in each tissue with specific composition of lignocellulose.

Keywords: Lignocellulose, Biomacromolecular mixture, Data mining

2. Materials and Methods.

Jatropha samples were collected from stem, seed and leaf. The stem was analyzed as whole tissues or divided in three parts: pith, xylem and bark (bark and phloem). The seed was divided in the internal part, kernel and the seed coat. These samples were dried and grind, low molecular weight metabolites were extracted using distilled water and 100% methanol. The seed samples were also treated with hexane to extract the oil. Than all samples were ball-milled for 12 hours with intervals of 10 minutes between 10 minutes of grinding. The ball-milled samples were dissolved in DMSO-d_6/pyridine-d_5 (4:1) [8] in the proportion of 80 mg of sample for 800 µL, however pith was dissolved in 20 mg for 600 µL.

These samples from different tissues were measured by 2D HSQC, HSQC-TOCSY and HSQC-NOESY using 700 MHz-NMR spectrometer. The central DMSO solvent peak was used as internal reference (δC 39.5, δH 2.49 ppm). The identification of the peaks was made using rNMR[9] and assignment reported from Kim & Ralph, 2010.

For the torrefaction experience the dried samples were grind and approximately 40mg was treated in different temperatures of torrefaction, 200 ℃, 250 ℃ and 300 ℃ in nitrogen gas flux and the residues were dissolved in 600 µL of DMSO-d_6/pyridine-d_5 (4:1) and measured by 2D HSQC using same spectrometer.

3. Results.

3.1. 2D HSQC.

Fig. 1 shows assignments of the polysaccharide anomeric region. We assigned the peaks related to polysaccharides as much as possible but there is numbers of peaks to be identified. In this analysis, it is possible to note difference in pattern of spectra of each tissue. (1-4)-β-D-glucopyranoside (1-4)-β-Glc*p*], cellulosic back bone, is present in all the tissues. Kernel showed the lowest quantity of signals, on the other hand pith has the largest. Seed coat

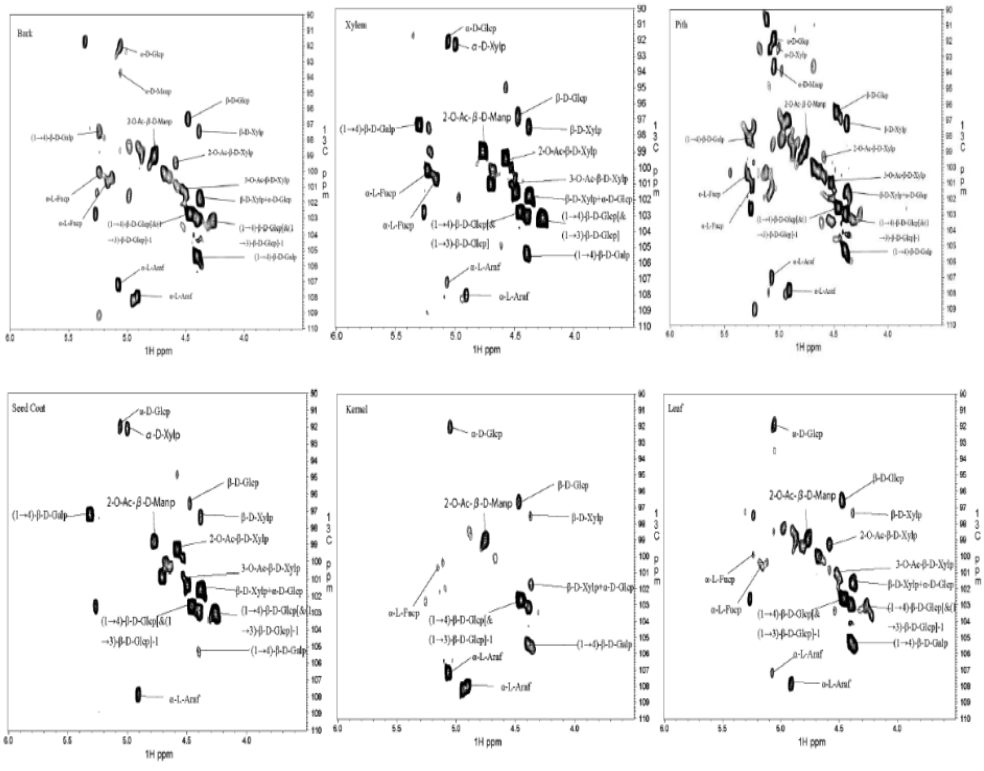

Fig. 1: Polysaccharide anomeric regions of 2D HSQC of each tissue, (1-4)- β-D-xylopyranoside [β-D-Xylp], (1-4)- β-D-glucopyranoside and (1-3)- ß-glucopyronoside [(1-4)&(1-3)- β-Glcp], α-L-fucopyranoside (α-L-Fucp), α-D glucopyranoside (α-D-Glcp), α-D xylopyranoside (α-D-Xylp), acetylated-β-D-mannopyranoside (2-O-Ac-β-D-Manp), acetylated-β-D-xylopyranoside (3-O-Ac-β-D-Xylp), acetylated-β-D-xylopyranoside (2-O-Ac-β-D-Xylp), 1-4)-ß-D-galactopyranoside [(1-4)- β-Galp], α-L-arabinofuranoside (α-L-Araf).

lacks α-L-fucopyranoside (α-L-Fuc*p*) and one of α-L-arabinofuranoside (α-L-Ara*f*) peaks which are found in all other samples. Bark, xylem and leaf have a similar pattern but some variation in the peak intensity.

3.2. 2D HSQC-TOCSY and NOESY.

We identified uncertain signals through the correlation in the 2D HSQC-TOCSY and 2D HSQC-NOESY. In the Fig. 2 the full lines represent the correlation present in TOCSY and NOESY analyses, the dotted lines represent the ones present just in NOESY. It was possible to identify acetylated xylopyranoside (2-O-Ac-Xyl*p*) carbon 1 (2-O-Ac-Xyl*p*-1) and carbon 2 (2-O-Ac-Xyl*p*-2), in the chemical shift 99.35/4.58 ppm and 73.25/4.65 ppm respectively, the correlation was present in NOESY and TOQSY. From the (1-4)-β-D-glucopyranoside [(1-4)-β-Glc*p*] (102.72/4.45 ppm) there are signals connecting peak in 79.95/3.49 ppm and 76.59/3.23 ppm, the signal in 72.92/3.03 ppm is also connected (1-4)-β-Glc*p*, but it is not possible to identify which carbon they represent, but 79.95/3.49 ppm or 72.92/3.03 ppm may be the carbon 2. From (1-4)-β-D-galactopyranoside carbon 1 [(1-4)- β-Gal*p*] in (105.42/4.39 ppm), it is possible to connect signals in 78.57/3.88 ppm, 78.20/3.55 ppm and 78.94/3.49 ppm, but it is not possible to identify which carbon it represent.

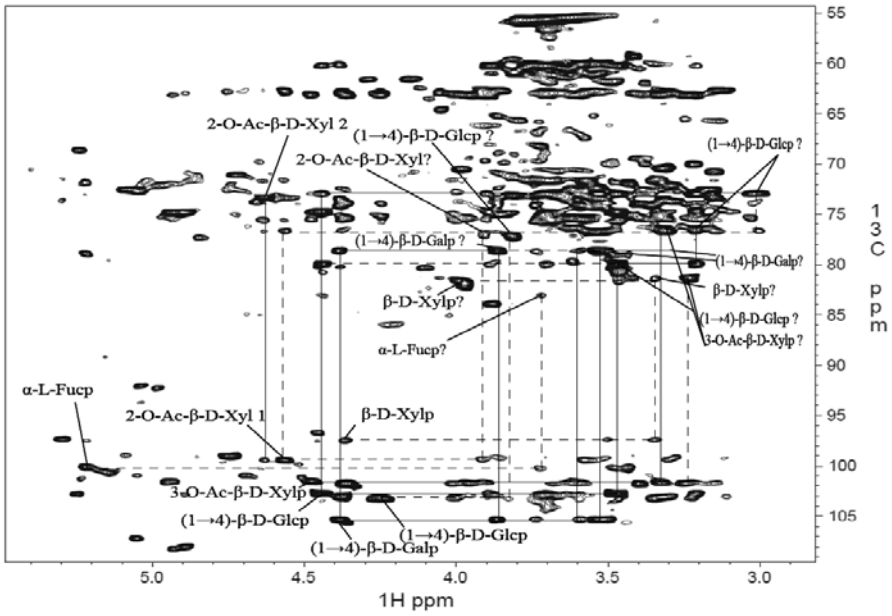

Fig. 2: Aliphatic and polysaccharide anomeric region of 2D HSQC-NOESY analysis, full lines correspond to the correlation present in 2D HSQC-TOCSY and 2D HSQC-NOESY, dotted line represent the correlation seen only in 2D HSQC-NOESY. The probable peaks identity using the correlation signals with (?) and some already identified without.

3.3. Quantification of lignin.

The HSQC intensity data from lignin were divided in two groups, compositions of monolignols and lignin substrutures. Its is notable the difference in the pattern of the each tissue. Stem is rich in S getting almost in 50%, followed by G with approximatly 30% and H with approximalty 20%. Bark, kernel and leaf have a simillar pattern of monolignol composition, S was not

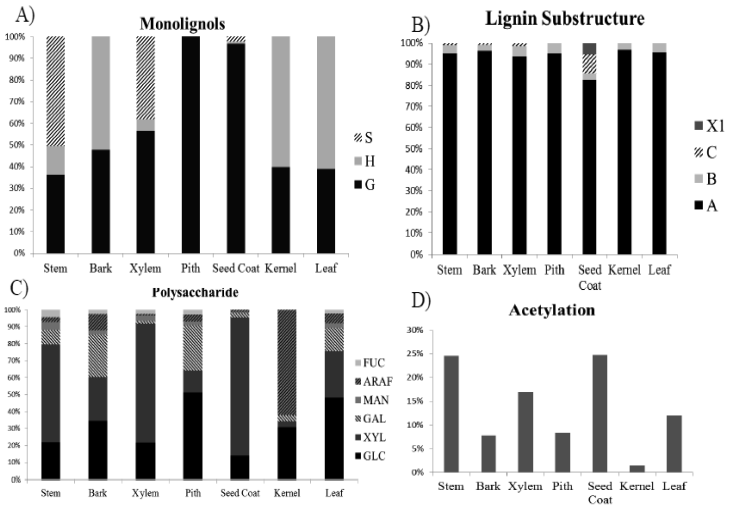

Fig.3 : A) Percentage of monolignols guaiacyl (G), syringyl (S) and *p*-hydroxybenzoates (H); B) Percentage of Lignin substructure β-O-4 (A), β-5 (B), β-β (C) and cinnamyl alcohol end group (X1); C) Percentage of polysaccharides derivated from fucose (FUC), arabinose (ARA), mannose (MAN), galactose (GAL), xylose (XYL), glucose (GLC); D) percentage of acetylated polysaccharides.

found however in kernel and leaf both are rich in H and bark in G. In pith the only monolignols found was G and seed coat is rich in G getting approximatly 95% and a small amount of S and H.

Analysis of lignin substructures, all the tissues have a large amount of A but there are some characteristics of different tissues. Stem, bark and xylem showed a simillar pattern of proportion of A, B and C, on the other hand pith, kernel and leaf are similar, with no presence of C and small amount of B. Seed coat showed a unique lignin substructure X1 and higher percentage of C than others (Fig.3).

3.4. Quantification of polysaccharides.

Polysaccharides were divided according to the derivate sugar: fucose (FUC), arabinose (ARA), mannose (MAN), galactose (GAL), xylose (XYL) and glucose (GLC). Pith, leaf and bark have similar constitution with 3 main polysaccharides GLC, XYL and GAL however bark have bigger percentage of ARAF and lower of GLC. Kernel showed a unique pattern with a large percentage of ARAF, followed by GLC, small amount of XYL and GAL but no presence of FUC and MAN.

The level of acetylation of the polysaccharides in each tissue was also analyzed, stem, xylem and seed coat present the highest levels followed by leaf, bark and pith, and the lowest was kernel.

3.5. Torrefaction.

The torrefaction experiments were made in different temperatures to analyze the effect in cellulose, hemicellulose and lignin degradation. The influence of the temperature in degradation levels in different components of the cell wall is remarkable, each tissue influenced differently according to the temperature (Data not shown).

4. Future perspectives.

The assignment of the peaks can advance with more analysis of 2D NMR techniques in different regions and it will increase the data base for future analysis. The pre-analysis of the tissue profiling showed interesting results, with different patterns, the profile can be more specific with new information from the assignments, giving more details of the composition of each tissue and though have a better view of the usage of each type of biomass.

References.

1. Kumar, A. and Sharma, S., (2008). An evaluation of multipurpose oil seed crop for industrial uses (*Jatropha curcas* L.): a review. Ind Crops Prod, 28: 1–10.
2. Manurung R., Wever D.A.Z., Wildschut J., Venderbosch R. H., Hidayat H., van Dam J. E.G., Leijenhorst E.J., Broekhuis A.A., Heeres H.J. (2009). Valorization of *Jatropha curcas L*. Plant parts: Nut shell conversion to fast pyrolysis oil.
3. Openshaw, K., (2000). A review of *Jatropha curcas*: an oil plant of unfulfilled promise. Biomass Bioenergy, 19: 1–15.
4. Gilbert H. J. (2010). The biochemistry and structural biology of plant cell wall deconstruction. Plant physiology, 153: 444-455.
5. Boerjan W., Ralph J. and Baucher M. (2003). Lignin biosynthesis. Annu. Rev. Plant Biology, 54 :519-546.
6. Balaskshin M., Capanema E., Gracz H., Chang H. and Jameel H. (2010). Quantification of lignin-carbohydrate linkages with high-resolution NMR spectroscopy. Planta, 233: 1097-1110.
7. Chen W.H., Kuo P.C. (2011). Torrefaction and co-torrefaction characterization of hemicellulose, cellulose and lignin as well as torrefaction of some basic constituents in biomass. Energy ,36: 803-811)
8. Kim H. and Ralph J. (2010). Solution-state 2D NMR of ball-milled plant cell wall gels in DMSO-d_6/pyridine-d_5. Organic & Biomolecular Chemistry, 8: 576-591.
9. Lewis I. A., Schommer S.C., Markley J. L. (2009). rNMR: open source software for identifying and quantifying metabolites in NMR spectra, *Magn. Reson. Chem*. 47, S123-S126

P-007

Y

A new approach for accurate quantification by using ^{19}F NMR

Taichi Yamazaki[1], Takeshi Saito[1] and Toshihide Ihara[1]
[1]National Institute of Advanced Industrial Science and Technology, National Metrology Institute of Japan

ABSTRACT

A new approach for accurate quantitative analysis using ^{19}F nuclear magnetic resonance (NMR) is discussed and presented. One of the most attractive and challenging properties of ^{19}F NMR for the quantification is its wide chemical shift dispersion. It is expected that off resonance effects of an excitation pulse is important to reveal the accuracy of the quantitative analysis. We propose three new methods to overcome the problem. Signal intensities, or peak areas, originating different functional groups of a molecule can be obtained 1 % or less with these methods. We have applied these methods to the independent resonances originating from two reference materials (RMs) to validate the purity determination processes. Variation of the signal intensities observed from the two RMs was proportional to each prepared concentration of the sample and the internal standard (IS); purity obtained with the methods agreed with the reference values of the RMs within their uncertainties.

1. INTRODUCTION

NMR spectroscopy has been widely used for structural determination of a molecule. Recently, application in quantification of the amount of substances using NMR has attracted attention, and quite a few papers have been published in quantitative NMR.

In ordinary quantitative analysis such as chromatographic techniques, a reference material of its own material is essential for accurate quantifications of sample purity. On the other hands, quantitative NMR (qNMR) technique does not require such a RM when an IS is added to the sample solution. The minimum requirement for the IS is as follows; does not react with the sample or solvents, or overlap to signal(s) from the other signals. The measurement accuracy is better to use an IS rather than an external standard. The influence of a time drift can be disregarded by using the IS. This method is a comparison of the number of nuclei, or it is traceable to the Internal System of Units. Therefore, NMR is a very useful analytical technique not only for the structural determination but also for the quantitative analysis.

While some research papers have been published on the qNMR with ^{1}H, few papers have discussed details of the accuracy of the quantifications of ^{1}H NMR[1),2)], but not for the applications in other nuclei such as ^{13}C, ^{15}N, ^{19}F and ^{31}P NMR. Therefore it is beneficial to reveal accuracy of quantification using other NMR active nucleus.

The fluorine compounds are widely used in engineering materials and probe molecules for biological activities pharmacological chemistry. ^{19}F NMR has been known as its wide chemical shift dispersion. This feature makes ^{19}F spectrum away from overlapping signals; however, this may be a source of problem for the accurate quantification because an excitation pulse may not be able to uniformly excite signals spread out such wide range of chemical shift.

In this presentation, we first discuss similarities and differences between ^{1}H and ^{19}F qNMR conditions in the view of measurement parameter settings; the T_1 was evaluated for optimization of measurement parameters; repeatability of signal intensities was evaluated. Then, relationship between intensity of a peak and the peak offset from excitation pulse, namely off resonance effect, are evaluated with two different excitation pulse angles. Based on the knowledge we obtained from the signal intensity variations, we propose a new approach for accurate ^{19}F qNMR. We applied these methods to quantification of purity of an analytical target using another molecule as an IS. Two reference materials whose purities had been certified were used for validating the purity determination processes. Finally, we discuss influence of data process on the purity.

2. EXPERIMENTAL

All ^{19}F NMR spectra were obtained Varian NMR Systems 600A (14.1 T) spectrometer. The probe used was a Varian's ^{15}N-^{31}P/^{1}H-^{19}F PFG dual-broadband probe. The temperature was regulated at 25 ^{o}C. Typical ^{19}F NMR experimental parameters were as follow; a 131578.9 Hz (233.1 ppm) spectral width, a 1.0 s acquisition time, 14.4 μs (π/2 (90 ^{o})) or 7.2 μs (π/6 (30 ^{o})) pulse widths, 32 scans and a 60 s pulse interval. All data processing was performed using MestReNova version 6.1. Range of integration was set to 150 Hz for both side from the peak evaluated unless sited.

Perfluorooctanoic acid potassium (PFOS-K) was obtained from Fluorochem. Chlorfenapyr, flusulfamide and diflubenzuron were obtained from Wako Pure Chemical Industries, Ltd. ("Traceable Reference Material" grade reference materials).

3. RESULTS & DISCUSSION

T_1 relaxation time was estimated for each peak independently. The T_1 was in the range of few seconds, which is similar to the T_1 of ^{1}H. Although T_2 was not evaluated, FID signal decays in much shorter time compare to the ^{1}H FID signal. Similar pulse interval and shorter acquisition time was chosen for ^{19}F qNMR parameter sets compare to the ^{1}H.

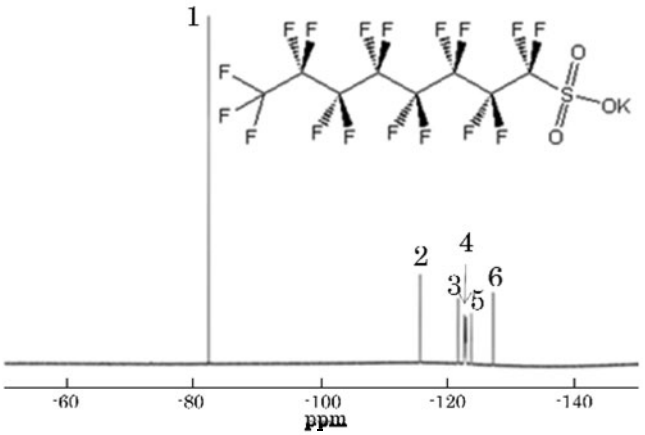

Figure 1. ^{19}F NMR spectrum of PFOS-K.

PFOS-K, shown in figure 1, was used to investigate off resonance effect. The further is the peak position from the offset, the lower the peak intensity is. Area of peaks 1 and 6 in the figure 1, which are 40 ppm apart, were different about 10 % and 2 % with 90^{o} and 30^{o} pulses, respectively. Figure 2 shows the results of offset array. The attenuation of peak intensity for the 90 ^{o} pulse was steeper where the signal offset became further from the peak. The excitation pulse did not give uniform peak intensities for such wide chemical shift range with the pulse width we used. The better measurement repeatability with an equal scan times was obtained with 90^{o} pulse because of the better signal to noise ratio.

Based on the evaluations, we propose three kinds of quantification methods for ^{19}F qNMR. The proposed methods are bellow;

【Method 1】 Set the offset frequency at the center of two signals of interest, these area are compared respects to the number of ^{19}F nuclei.

【Method 2】 Run two sets of experiments with each of the offset frequency set to the vicinity of the peak of interest. Areas of each of the vicinity peaks are compared.

【Method 3】 Observe two sets of experiments identical to the method 2. Areas of each peak from two spectra are added; the two added areas are compared.

Influence of off resonance effect could be disregarded with all suggested methods.

Table 2. The result of quantification of intra-molecular analysis with method 1.

Analytical target			IS			
Peak No.	the number of F	Area/ the number of F (A)	Peak No.	the number of F	Area/ the number of F (IS)	(A/IS) × 100 %
1	3	18251	2	2	18093	0.86
1	3	18147	3	2	17986	0.88
1	3	18126	5	2	18160	0.19
1	3	18064	6	2	18039	0.14
2	2	18230	6	2	18081	0.81

Results of the method 1 using two the peaks from PFOS-K as an analytical target and an IS peaks, respectively, is shown in Table 2. The results indicated that the method with 90 ^{o} pulse enables to evaluate the peak intensities less than 1 % of variations. Although not shown here, the method with 30 ^{o} pulse was within 2 % of variations. The difference of variations between these two pulse angles was caused by signal to noise ratio of each peak. The other methods show similar to the results of the method 1. These methods are suggested to have enough capability in accurate quantification.

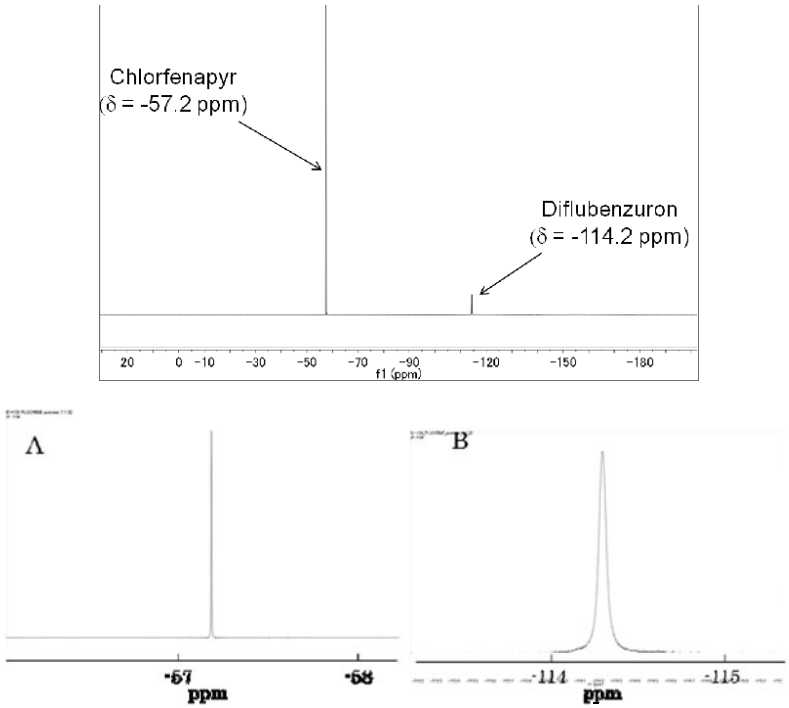

Figure 3. ^{19}F NMR spectrum of chlorfenapyr and Diflubenzuron (upper). Expanded ^{19}F NMR spectrum of chlorfenapyr and Diflubenzron (under,A:chlorfenapyr, B:diflubenzuron).

For expanding the method within a molecule to comparison of two peaks from two different molecules, purities of flusulfaamide and diflubenzuron, as analytical targets, were determined by these methods using Chlorfenapyr as the IS. Since these three molecules are reference materials with their purities certified, the certified values are obtained if the methods work as expected. In the case of flusulfaamide as an analytical target, purities obtained with these methods were agreed with the reference value within its limit of uncertainty. However, in the case of diflubenzuron, the purities were not corresponded with the reference value. In the former case, full-width of half maximum (FWHM) of the analytical target and the IS were in a similar range. The latter case, the line widths were quite different. The line width at the FWHM of diflubenzuron was about 17 times of that of the IS peak (Figure 3). Broader peak need a care for adjusting range of

integration because of its peak shape. Integration range was defined based on the FWHM of each peak. When such a integral range was selected, purities obtained for diflubenzuron were agreed with the reference value within its limit of uncertainty (Figure 4).

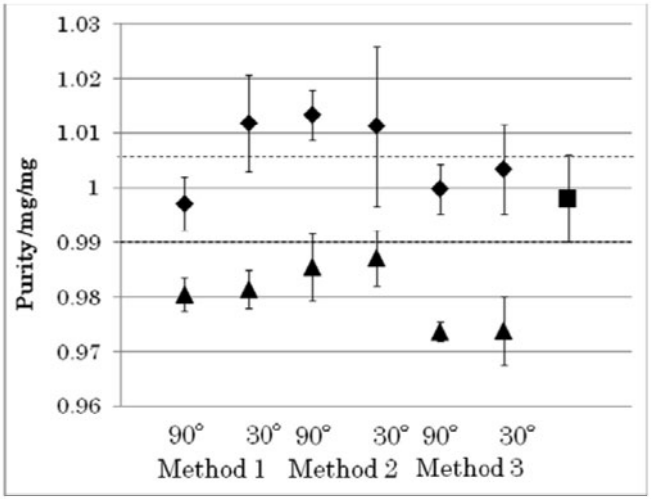

Figure 4. ▲:integral range is 150 Hz from signal center. ◆:integral range is 20 times to the FWHM. ■:a reference value.

4. Conclusions

We propose three different methods for accurate quantification using ^{19}F NMR. These methods overcome problems on the off resonance effect. For the broad peaks, care for setting integration range is required; with wider range based on their FWHM, accurate quantitative results are obtainable. These proposed methods can be extended to other NMR active nuclei with wide chemical shift dispersions for the accurate quantifications.

REFERENCE

1)Saito T, Nakaie S, Kinoshita M, Ihara T, Kinugasa S, Nomura A, and Maeda T (2004) Metrologia, 41:213-218.

2)Saito T, Ihara T, Koike M, Kinugasa S, Fujimine Y, Nose K, and Hirai T, (2009) Accred Qual Assur, 14:79-86.

^{19}F NMR, quantification, off resonance effect

P-008 A novel sensitivity enhancement technique for solution NMR utilizing long longitudinal relaxation time

Kyoko Furuita[1], Yoshikazu Hattori[1], Takahisa Ikegami[1], Toshimichi Fujiwara[1] and Chojiro Kojima[1, 2]
[1]Institute for Protein Research, Osaka University
[2]Graduate School of Biological Sciences, Nara Institute of Science and Technology

ABSTRACT

NMR experiments of the molecules with long longitudinal relaxation time require long measurement time because long repetition delays are necessary. We have developed a novel sensitivity enhancement method by contrast utilizing long longitudinal relaxation time. This method is based on the double-acquisition method previously developed by M. Fukuchi *et al.*. In this study, we have successfully applied this method to ^{1}H-^{13}C HSQC and ^{1}H-^{15}N HSQC experiments of proteins.

INTRODUCTION

Macromolecules at a high magnetic field or small molecules have long longitudinal relaxation time. Therefore, long repetition delays, i. e., long measurement time, are required to obtain their NMR spectra. Here, we have developed a novel sensitivity enhancement method that utilizes such long longitudinal relaxation time. In this method, free induction decay (FID) signals are acquired twice within a single scan. The concept of acquisition of two FID signals within a single scan was firstly introduced many years ago[1)], afterward some similar pulse schemes were proposed to obtain different types of spectra in one experiment, or to increase sensitivity. The latter usage of this acquisition method has been recently developed by M. Fukuchi *et al.*[2)], and called double-acquisition method, where a set of two quadrature data can be obtained in a single scan. When two FID signals are acquired within a single scan to obtain different types of spectra or to enhance sensitivity, secondly acquired components should be stored along z-axis during the first acquisition in order to prevent disappearance of detectable signals due to transverse relaxation. However, the requirement mentioned above is generally fulfilled when In-Phase (IP) and Anti-Phase (AP) signals are acquired within a single scan. In this study, we applied the double-acquisition method to ^{1}H-^{13}C HSQC and ^{1}H-^{15}N HSQC experiments by acquiring IP and AP signals.

MATERIALS & METHODS

All experiments ware performed on Bruker AVANCE 800 spectrometer. Data ware processed by TOPSPIN 2.1 (Bruker) and NMRPipe, and analyzed by NMRPipe and Sparky 3.115. The NMR sample of benzen was prepared by mixing 6 μl of benzen and 594 μl of CD_3OD. The NMR sample of ubiquitin (E34S) was prepared at a concentration of 1.0 mM in 10/90% H_2O/D_2O containing 50 mM HEPES and 50 mM NaCl.

sensitivity enhancement, high magnetic field, longitudinal relaxation

RESULTS & DISCUSSION

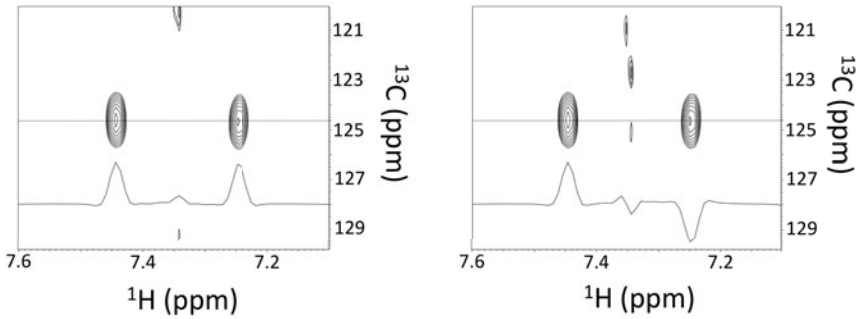

Figure 1. IP (left) and AP (right) spectra obtained by ^{1}H-^{13}C dfHSQC experiment of benzen. 1D slices corresponding to the horizontal lines are shown.

The double-acquisition method was applied to fast HSQC experiment. The experiment is named double-acquisition fast HSQC (dfHSQC) herein. The dfHSQC experiment utilizes both single- and double-quantum terms that are created at the end of the evolution period; the single-quantum term is detected as IP signals, while double-quantum term is detected as AP signals.

First, ^{1}H-^{13}C dfHSQC experiment was developed using benzen. IP and AP spectra were successfully measured (Figure 1). ^{1}H-^{15}N dfHSQC experiment was developed using a protein, ubiquitin (E34S). IP and AP spectra were successfully measured.

In order to evaluate the performance of the double-acquisition method applied to HSQC, peak intensities in dfHSQC spectra were compared with those in WATERGATE-HSQC with water flip-back pulse (WG-HSQC), fast HSQC (fHSQC), and gradient sensitivity enhanced HSQC (SE-HSQC) spectra (Figure 2). In the case of benzen, the peak intensity in dfHSQC almost doubled compared with WG-HSQC and fHSQC. In the case of ubiquitin (E34S), the peak intensity in dfHSQC was improved compared with WG-HSQC and fHSQC, but the improvement was smaller compared with benzen. This is probably because the longitudinal relaxation time of ubiquitin (E34S) is shorter than that of benzen, hence secondly acquired signals of ubiquitin (E34S) were more attenuated during first acquisition. Peak intensities of dfHSQC spectra for both benzen and ubiquitin (E34S) were similar to those of their SE-HSQC spectra. It is because that the double-acquisition method is an alternative to the sensitivity enhancement method.

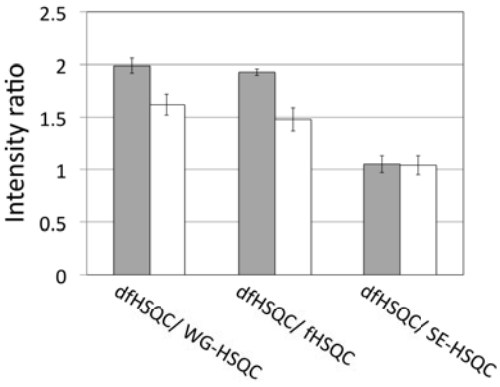

Figure 2. Peak intensity ratios of dfHSQC to other HSQC of benzen (gray bars) and ubiquitin (E34S) (open bars).

In this study, we showed that the double-acquisition method is successfully applied at least to ^{1}H-^{13}C HSQC and ^{1}H-^{15}N HSQC experiments by acquiring IP and AP signals. The dfHSQC experiment will be effective in observing large protein at a super high magnetic field and molecules in solid state, as well as small molecules as demonstrated here.

REFERENCES

1) Haasnoot, C.; Vandeven, F.; Hilvers, C. *Journal of Magnetic Resonance* **1984**, 343.
2) Fukuchi, M.; Inukai, M.; Takeda, K.; Takegoshi, K. *Journal of Magnetic Resonance* **2008**, 300.

P-009 Structural and dynamic studies of proteins in living cells by in-cell NMR spectroscopy

Jumpei Hamatsu[1], Takahiro Shirai[1] Daniel Nietlispach[2], Teppei Ikeya[1], Masaki Mishima[1], Masahiro Shirakawa[3], and Yutaka Ito[1]

[1]Department of Chemistry, Graduate school of Science & Engineering, Tokyo Metropolitan University;
[2]Department of Biochemistry, University of Cambridge;
[3]Department of Molecular Engineering, Graduate school of Engineering, Kyoto University

Abstract

In-cell NMR is the only available method for investigating detailed structure and dynamics of proteins at work inside living cells. In this presentation, we report our recent in-cell NMR studies of proteins focusing on identifying protein structure and dynamics in living cells. We performed ^{15}N-relaxation experiments by in-cell NMR to elucidate dynamic properties of proteins in cellular environment. In addition, we will report our recent trial experiments on heteronuclear multidimensional NMR studies of proteins in living eukaryotic cells.

Introduction

In living cells, a variety of soluble macromolecules such as proteins, DNAs and RNAs are exist under very crowded environment. The total concentration of these macromolecules is the range of 300 ~ 400 g/L and its occupancy reaches to 30 ~ 40 % of the cytosol[1]. Such a crowded environment influences the kinetics and thermodynamics of protein folding, protein-protein interaction, and ligand-binding events by the exclude volume effects. Therefore, in order to understand the detail of structures and dynamic properties of cytosolic proteins, it is necessary to collect information under physiological condition.

In-cell NMR has been used to detect various intracellular events such as conformational exchanges, dynamics and binding events in living bacterial cells. We also reported our in-cell NMR study of the protein structure determination in living *E. coli* cells[2]. In eukaryotic cells, in-cell NMR studies have been performed by injecting proteins into *Xenopus laevis* oocytes or eggs[3,4]. Recently cell-penetrating peptides[5] and the pore-forming toxin streptolysine O (SLO)[6] have been used to deliver proteins that can be observed in living mammalian cells. However, for the low sensitivity due to the limited intracellular concentration of target proteins, only 2D NMR-based approaches have been so far available for in-cell NMR studies using eukaryotic cells.

Here we report our recent in-cell NMR works of some model proteins on identifying protein structure and dynamics in living prokaryotic and eukaryotic cells.

Results

In-cell NMR in living E. coli cells

We have used the *Thermus thermophilus* HB8 protein TTHA1718 as a model system. ^{15}N-T_1, T_2

Key words: In-cell NMR, protein structure, protein dynamics

values of TTHA1718 in living *E. coli* cells and *in vitro* have been collected. Significant differences were observed between the ^{15}N-T_1, T_2 values from in-cell NMR and *in vitro* experiments. Especially, ^{15}N-T_2 values obtained from in-cell NMR experiments were significantly short when compared with those *in vitro*. To verify chemical exchange contribution to the transverse relaxation rate (R_{ex}), we measured TROSY selected spin-echo experiments by in-cell NMR. Obtained R_{ex} values suggests that there is no significant exchange contribution to the ^{15}N-T_2 relaxation in living *E. coli* cells (Fig. 1).

Similar ^{15}N-relaxation analysis is in progress on the B1 domain of streptococcal protein G (GB1), which may provide us a clearer image of the general effects of the cellular environment to the protein dynamics.

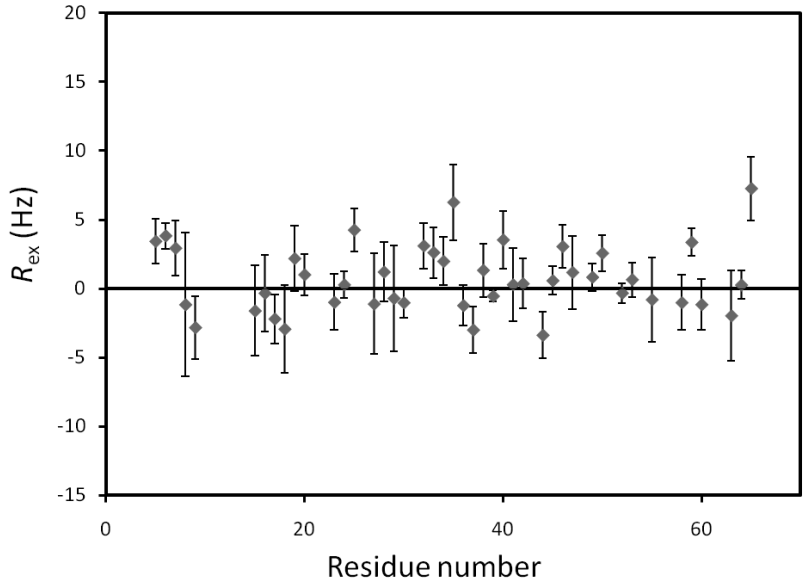

Fig.1
Chemical exchange contributions to the transverse relaxation rate of TTHA1718 protein in living *E. coli* cells derived from TROSY selected spin-echo experiments are plotted as a function of the residue number. The data was collected at 600 MHz using Bruker AVANCE 600 spectrometer with a triple resonance cryoprobe. Experiment was repeated 5 times for statistical analysis. Error bars indicate SD from 5 independent measurements.

In-cell NMR in living Sf9 cells

Sf9 cultured insect cells are widely used for protein production in eukaryotic cells. As another demonstration of eukaryotic in-cell NMR, we selected sf9 system and tried to observe in-cell NMR spectra of overexpressed target proteins. Baculoviruses encoding either TTHA1718 or GB1 genes were constructed and inoculated into sf9 cells. Protein expression was performed in ^{15}N-labelled growth medium. For both TTHA1718 and GB1 cases the 2D ^{1}H-^{15}N HSQC spectra measured on sf9 samples showed well resolved cross-peaks originate from target proteins, suggesting the potential usefulness of sf9 protein expression system in extending eukaryotic in-cell NMR approaches.

References:

[1] Ellis, R. J. *Trends Biochem. Sci.* 26, 597-604(2001) **[2]** Sakakibara, D. et al. *Nature.* 458, 102-105(2009) **[3]** Selenko, P. et al. *Proc. Natl. Acad. Sci. USA.* 103, 11904-11909 (2006) **[4]** Sakai, T. et al. *J. Biomol. NMR*. 36, 179-188 (2006) **[5]** Inomata, K. et al. *Nature.* 458, 106-110 (2009) **[6]** Ogino, S. et al. *J. Am. Chem. Soc.* 131, 10834-10835 (2009)

P-010 Protein Modification Method for Studying Protein-Protein Interaction by NMR

Yoshikazu Hattori[1], Izuru Ohki[2], Kyoko Furuita[1], Takahisa Ikegami[1], Harumi Fukada[3], Masahiro Shirakawa[4], Kei-ichi Yokoyama[5], Ei-ichiro Suzuki[1,5], Toshimichi Fujiwara[1], Chojiro Kojima[1,2]
[1]Inst. for Protein Res., Osaka Univ., [2]Grad. Sch. of Biol. Sci., NAIST, [3]Grad. Sch. of Life Env. Sci., Osaka Pref. Univ., [4]Grad. Sch. of Eng., Kyoto Univ., [5]Inst. for Innovation, Ajinomoto Co. Inc.

ABSTRACT

NMR is a powerful tool for studying protein-protein interactions. This method requires the stable isotope labeling such as $^{13}C/^{15}N$-enrichment. Protein modification is one of the easiest ways for such labeling. Here we applied chemical and enzymatic protein modification methods to studying protein-protein interactions. As the chemical labeling technique, ^{13}C-methylation of lysine was applied to the determination of the interaction sites for ubiquitin. As the enzymatic labeling technique, ^{15}N-exchange of glutamine using microbial transglutaminase has been examined. These methods were useful to analyze protein-protein interactions.

INTRODUCTION

NMR spectroscopy has an ability to detect protein-protein interactions at atomic resolution under physiological conditions. The detection is enabled by the incorporation of stable isotopes such as ^{13}C and ^{15}N into proteins. Stable isotope labeling methods rely almost on recombinant expression systems, but they are not suitable for the production of many biologically important targets such as transmembrane proteins and extracellular proteins.

Protein modification is a useful way of stable isotope labeling for purified proteins. Lysine methylation is a well-established chemical modification technique, which can add two methyl groups into an amino group of lysine under the mild condition (neutral pH, 4 °C). Thus ^{13}C-methyl groups can be incorporated by using a ^{13}C-enriched reagent (Figure 1A). This method had been applied to studying protein-nucleic acid, protein-metal ion and protein-small ligand interactions. In this study, it was applied to the detection of protein-protein interactions between ubiquitin and its interacting factor.

Another way of protein modification is enzymatic modification. Microbial transglutaminase (MTG) catalyzes the formation of covalent bonds between glutamine γ-carboxyamide groups and lysine ε-amino groups. In the presence of excess ^{15}N-enriched ammonium salt, ^{15}N-exchange reaction of glutamine γ-carboxyamide groups proceeds (Figure 1B). In this study several proteins were ^{15}N-exchanged and the information about protein-protein interactions was obtained.

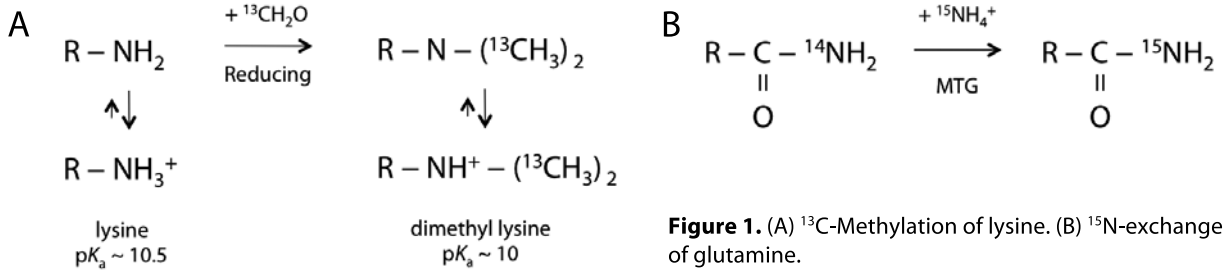

Figure 1. (A) ^{13}C-Methylation of lysine. (B) ^{15}N-exchange of glutamine.

Protein Modification, Lysine, Glutamine

MATERIALS & METHODS

^{13}C-methylation of lysine was performed using dimethylamine borane as a reductant and ^{13}C-formaldehyde as a ^{13}C source, and the regents were removed by dialysis or desalting column. ^{15}N-exhcahnge of glutamine was performed using MTG produced by Ajinomoto Co. Inc. and ^{15}N-ammnonium chloride as a ^{15}N source.

RESULTS & DISCUSSION

^{13}C-methylation of lysine

Ubiquitin was completely di-methylated at its lysine and N-terminal amino groups, and the NMR signals of methyl groups were measured using ^{1}H-^{13}C HSQC experiments. The assignments were achieved by substituting each lysine with arginine.

As the protein YUH1, known as an ubiquitin C-terminal hydrolase, was added to methylated ubiquitin, the signals of methyl groups were changed specifically (Figure 2A). Referring to the crystal structure of the complex of ubiquitin and YUH1, the chemical shift changes of the methyl groups in the binding surface were found to be significant (Figure 2B).

The interaction between ubiquitin and YUH1 was further analyzed by other ways to compare it before and after methylation. ITC experiments indicated similar dissociation constants. ^{1}H-^{15}N HSQC experiments suggested the chemical shift changes of the ubiquitin backbone amide groups were well correlated.

These results indicate that ^{13}C-methylation of lysine does not cause marked changes in the binding affinity and surface, and that ^{13}C-methyl groups added to lysine can be used to determine protein-protein interaction sites.

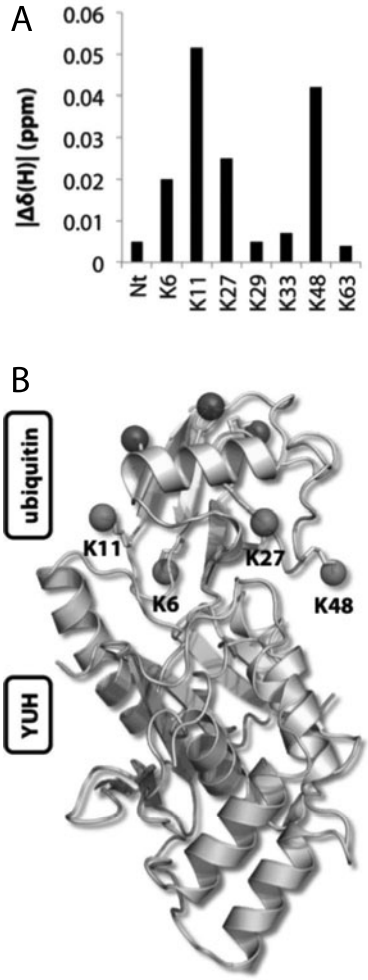

Figure 2. (A) Proton chemical shift changes of ubiquitin methyl groups by the addition of YUH1. (B) Lysines with significant chemical shift changes shown in the crystal structure of the complex of ubiquitin and YUH1 (PDBID 1CMX).

^{15}N-exchange of glutamine

Several proteins (ubiquitin, FKBP12, BSA, lysozyme, YUH1 and GF14b) were mixed with MTG and ^{15}N-ammonium chloride, and ^{1}H-^{15}N HSQC experiments were performed. Although some peaks were detected for FKBP12, BSA, YUH1 and GF14b, no peak was detected for ubiquitin and lysozyme. This may be related with solvent accessibility and surface charge, but the correlation was not clear.

To study protein-protein interactions, YUH1 was mixed with MTG and ^{15}N-ammonium chloride in the presence of ubiquitin. In this case, the intensity of a specific peak was significantly decreased. For the assignment of this peak, Q153 located in the binding surface, was mutated to asparagine.

The substrate specificity of MTG may be related to the ^{15}N-exchange reactivity of each glutamine residue. Therefore, the modifications of MTG may increase its availability.

P-012 Uniform and Site-specific ^{13}C-labeling in Proteins Using Plant BY-2 Cells with Inducible Virus Vectors

Makoto Takeuchi[1], Masashi Mori[2,3] and Shin-ya Ohki[1,3]
[1]Japan Advanced Institute of Science and Technology
[2]Ishikawa Prefectural University
[3]JST-SENTAN

We have successfully prepared ^{15}N- and ^{13}C-labeled proteins using the BY-2 protein expression system that requires sucrose as the sole carbon source. As the alternative of expensive ^{13}C-sucrose, workability of some cost-effective ^{13}C-labeled chemicals was tested. Here we report the utilities of uniform and site-specific ^{13}C-glucose, amino acids, and metabolites in this system. It was found that various carbon sources, which had not been examined, can be employed for our plant BY-2 protein expression system.

INTRODUCTION

Although *E. coli* protein expression systems are easy to handle, they have some disadvantages to express eukaryotic proteins. Therefore, the other protein expression systems have been examined. In this context, we previously reported a novel protein expression system using suspension-cultured tobacco BY-2 (Nicotiana tabacum cv. Bright yellow 2) cells with inducible virus vectors. This BY-2 system effectively produces several mg samples from 30 – 50 mL culture medium, and is possible to obtain proteins containing disulfide bonds with their proper conformations.

In the previous paper, we only reported uniform ^{15}N-labeling [1]. It is known that BY-2 cell requires sucrose as the sole carbon source. This seems disadvantage for ^{13}C-labeling, because ^{13}C-labeled sucrose is expensive. Thus, we examined the utility of glucose, amino acids, and metabolites (α-keto acids). In this presentation, we show several procedures to achieve the uniform and site-specific ^{13}C-labeling in proteins using the BY-2 system.

MATERIALS AND METHODS

Protein expression. The protein expression and purification were performed by the methods reported previously [1]. BPTI, containing three disulfide bonds, was employed as the model sample. Instead of the unlabeled sucrose, the uniformly ^{13}C-labeled sucrose, sucrose in which glucose or fructose unit is labeled with ^{13}C, or uniformly ^{13}C-labeled glucose was dissolved in the culture medium. For the selective-labeling, ^{13}C-labeled amino acids or metabolites were added to the standard culture medium.

Dry weight measurement. The cells grown at various different conditions were collected and lyophilized. Weight of the dried cells was measured to assess the growth level.

Protein expression level. To compare protein expression level, the density of bands on the SDS-PAGE gel was analyzed using ImageJ image analysis software (http://rsb.info.nih.gov/ij/).

NMR experiments. The labeled BPTI was dissolved into 20 mM phosphate buffer containing 100 mM KCl adjusted at pH 5.8 with direct reading of a pH meter. The solvent contained 10 % D_2O for NMR lock. The NMR data were recorded on a Bruker Avance III 800 equipped with a TCI-cryogenic probe. All NMR experiments were performed at 25 ^{o}C. The data

Plant cell, ^{13}C-labeling, metabolite

were processed and displayed with NMRPipe.

RESULTS AND DISCUSSION

Sucrose. We successfully obtained uniform $^{13}C/^{15}N$-labeled BPTI. The labeling rate was estimated as > 90 %. The result of HNCA will be shown in the presentation.

Sugar-specific labeled sucrose. The ^{13}C-labeling rate of all carbon sites was estimated as the peak intensity in ^{1}H-^{13}C CT-HSQC. When the sucrose, in which glucose unit is labeled with ^{13}C, was employed as the sole carbon source, it was found that ^{13}C-labeling rate of Ile γ1 and γ2, and Leu δ1 and δ2 in the product protein, BPTI, is effectively reduced, for example. In the presentation, all results of such reduction will be summarized.

Glucose. We examined the utility of glucose as the sole carbon source in the culture medium. We optimized the amount of glucose as 15 g/L. Although the amount of cells harvested from the glucose medium is approximately 10 % of that obtained in the standard procedure, the amount of expressed BPTI was almost identical. We obtained uniform ^{13}C-labeled BPTI, and observed the NMR data showing applicability of ^{13}C-glucose in the BY-2 system. In the poster presentation, we will also discuss the utility of site-specific ^{13}C-labeled glucose.

Branched hydrophobic amino acids. We found that addition of Val, Leu, or Ile (100 mg/L each) to the standard culture medium does not inhibit the BY-2 cell growth. Therefore, we tried to express BPTI using culture medium containing ^{13}C-labeled Val, Leu, or Ile. Figure 1 shows that the NMR data of the purified proteins contain ^{13}C-labeled Val, Leu, or Ile. The NMR data show the added amino acids are used for the cell growth and protein expression. Val, Leu, and Ile are thought to be located downstream of metabolism, and thus the scrambling of ^{13}C to the other amino acid types is not so serious. It was found that both Val and Leu are labeled, when ^{13}C-Val was supplied in the culture medium. The result is caused by metabolic scrambling, but the inverse isotopic dilution from Leu to Val was negligible, similar to the *E. coli* system.

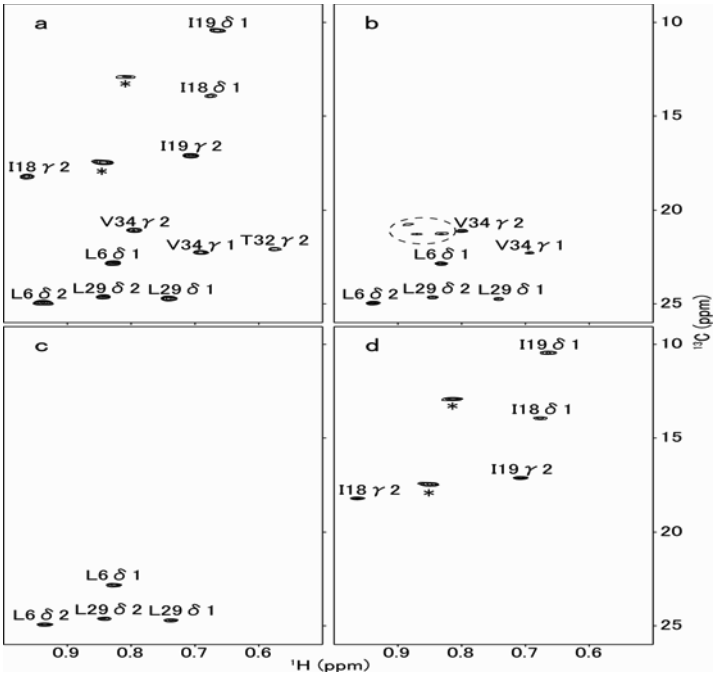

Figure 1. Methyl region of ^{1}H-^{13}C CT-HSQC of BPTI. The constant time (CT) was set as 27 msec for all experiments. The samples were prepared in the culture medium containing (a) UL-^{13}C, (b) ^{13}C-Val, (c) ^{13}C-Leu, and (d) ^{13}C-Ile. The peaks are labeled with amino acid type and residue number. Asterisks represent the peaks of the tag sequence. In panel b, peaks in the circle with dotted line are resonating from impurity.

The results suggest that addition of Val, Leu, or Ile is easily adopted for the preparation of site-specific [^{13}C-methyl]-labeled Val, Leu, and Ile residues in NMR samples, when the site-specific [^{13}C-methyl]-labeled amino acids are employed.

Metabolites. We will also report the workability of ^{13}C-labeled metabolites for preparation of the methyl-specific ^{13}C-labeled proteins in the BY-2 system.

REFERENCE

1. Ohki S, Dohi K, Tamai A, Takeuchi M, Mori M (2008) Stable-Isotope Labeling using an Inducible Virus Vector and Suspension Cultured Plant Cells. *J. Biomol. NMR* 42: 271-277.

P-013 Sampling strategy for plant biomass from hydrosphere

Kengo Ito [1], Kenji Sakata [1], Yasuhiro Date [1,2], Jun Kikuchi [1,2,3,4]

[1]Grad. Sch. Nanobio., Yokohama City Univ., [2]RIKEN Plant Sci. Cent., [3]Biomass Eng. Prog., RIKEN Res. Clust. Innov., [4]Grad. Sch. Bioagri., Nagoya Univ.

Abstract

Plant biomass is attractive resources for renewable energy and materials. However, little information of plant biomass from hydrosphere is available compared to land plants. Especially, although extraction method for NMR measurement to characterize the biomass component in land plant has already developed, plant biomass from hydrosphere is not able to characterize by similar method with land plant. Therefore, we attempted to develop the extraction methods for characterization of plant biomass from hydrosphere by modification of the conditions for solubility and extraction procedure.

Introduction

Biomass resources originated from plants have been received increasing attention as renewable feedstock in recent years. Plant biomass consisted mainly of cellulosic biomass does not compete with food, and enable us to provide a sustainable human development based on carbon neutral concept. In the recently progress for the plant biomass research, many researchers have been started to provide the information for compositions, structures and characteristics of cellulosic biomass in land plants. Especially, the compositional variations for cellulosic biomass in land plants were successfully characterized by using NMR profiling method based on DMSO/pyridine solvent systems in combination with removing of low-molecular compounds (1). However, little information of plant biomass from hydrosphere is available compared to land plant because plants from hydrosphere have different structures and compositions of biomass. Therefore, we attempted to develop the extraction methods for characterization of plant biomass from hydrosphere by modification of the conditions for solubility and extraction procedure.

Experimental methods

In this research, extraction procedures and conditions for plant biomass from hydrosphere were examined by various methods such as chemical and physical pretreatments, temperature conditions, ultrasonication and solvent systems. Samples used in this study were collected from Aburatsubo and Tenjinjima in Kanagawa, Japan. The collected samples classified into brown algae were freeze-dried, crashed, and processed into particle size by physical pretreatments such as ball-milling and Automilling. The solvents for extraction we examined were D_2O, CD_3OD and DMSO-d_6/pyridine-d_5. The all extracted samples were measured by 500 MHz-NMR spectrometer. The obtained data were processed by binning, digitizing, and evaluating with multivariate statistical analysis such as principal components analysis (PCA) using program R.

Keyword: Plant biomass, sampling strategy, hydrosphere

Results and Discussion

The brown algae samples were extracted by methanol, D_2O and DMSO/pyridine solvent (as shown in Fig. 1). The spectra derived from semipolar metabolites were detected in the NMR data by methanol extraction. The spectra derived from small molecules and water soluble polysaccharides were detected in the fraction of D_2O solvent. On the other hand, other residual polysaccharides such as cell wall fraction were solubilized by DMSO/pyridine solvent. Therefore, our developed sampling procedures were capable of removing the lipids and some low-molecular metabolites by methanol solvent, removing water soluble polysaccharides and other small molecules by D_2O, and extracting the cell wall fraction in plant biomass from hydrosphere by DMSO/pyridine solvent.

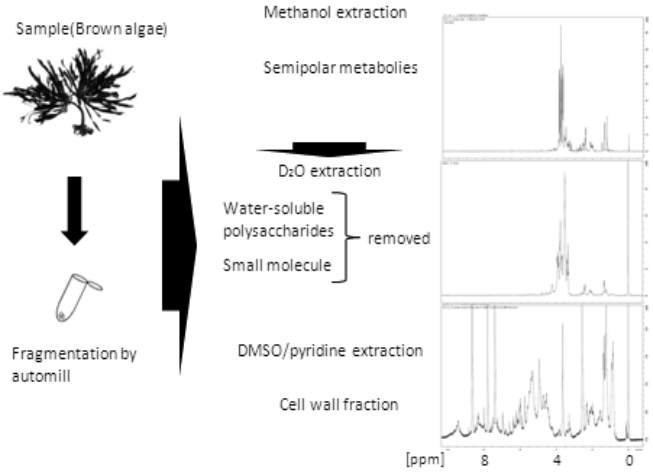

Fig.1 Sampling strategy with evaluation of ^{1}H-NMR spectra (brown algae)

In addition, NMR spectra by methanol extraction of brown algae were evaluated by PCA score plots and loading plot (Fig. 2). The profiling data of brown algae were clearly separated according to the differences based on extraction processes, conditions and procedures. Methanol extraction without removing processes of methanol and D_2O solvents was observed the high signal intensities near 3.7 ppm in loading plots analysis. On the other hand, the methanol extraction with D_2O removing process without methanol removing process was capable of extraction for the only semipolar metabolites from brown algae biomass. Therefore, our sampling strategy for algae biomass was possible to characterize the target metabolites from low-molecular compounds and semipolar metabolites to insoluble biomass by changing the solvent system and extraction procedures.

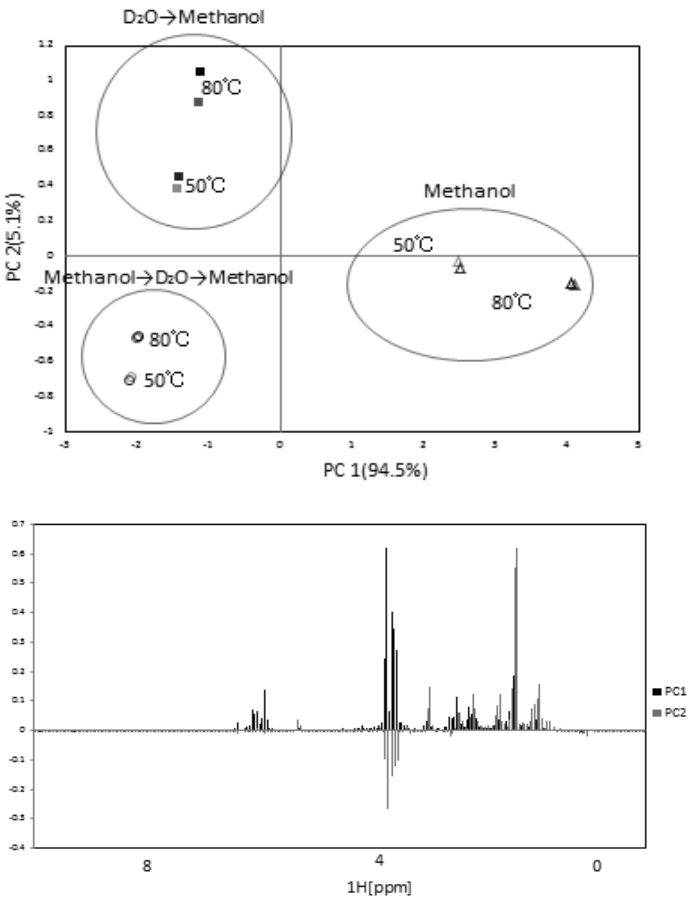

Fig.2 PCA score plot and loading plot (methanol extraction of brown algae).

References: (1)Hoon Kim and John Ralph, *Org. Biomol. Chem.*, 2010, **8**, 576-591

P-014 Y

Strategy for suppression of aggregation in FROUNT, a regulator of chemokine receptor

Tatsuichiro Tsuji[1], Sosuke Yoshinaga[1], Kaori Esaki[1], Yuya Terashima[2,3], Etsuko Toda[2], Kouji Matsushima[2] and Hiroaki Terasawa[1]
[1]Grad. Sch. Pharm. Sci., Kumamoto Univ.,
[2]Grad. Sch. Med., Univ. Tokyo, [3]ECI, Inc.

[Abstract]

Protein aggregation is often a serious problem when researching proteins for the field of structural biology. We established an NMR-based method to elucidate aggregation sites and identified the residues involved in the aggregation of the C-terminal domain of FROUNT (FNT-C). We carried out mutagenesis, obtaining a stably monomeric mutant, which gave intense NMR signals and retained the CCR2-binding activity.

[Introduction]

Aggregation induces NMR line-broadening which leads to the disappearance of NMR peaks. Suppression of aggregation has been conducted by various methods. For example, screening of many solution conditions is utilized for to obtain the optimal sample conditions [1]. Another strategy is to replace surface-exposed hydrophobic residues with charged residues or glycine using known structures with high structural homology [2]. We identified a cytoplasmic protein FROUNT, which binds to a chemokine receptor CCR2 and mediates intracellular signaling [3]. The C-terminal domain of FROUNT (FNT-C) specifically and directly interacts with the C-terminal region of CCR2. NMR analyses showed that FNT-C forms aggregates in solution. In this study, we obtained a stably monomeric mutant, which retained the CCR2-binding activity, by site directed mutagenesis of the aggregation sites.

[Materials and methods]

The FNT-C protein was expressed in *Escherichia coli* BL21 cells transformed with the pGEX-4T-3 plasmid that encodes FNT-C DNA. FNT-C was purified through GS4B-affinity chromatography and ion exchange chromatography. The aggregation state of FNT-C and mutant proteins was confirmed by dynamic light scattering (DLS) and gel-filtration chromatography. We performed triple resonance NMR experiments and calculated secondary structure propensity using the SSP method [4]. We conducted NMR experiments at various protein concentrations. NMR titration experiments were performed by addition of a hydrophobic compound to the FNT-C solution. The CCR2-binding activity of the mutants was evaluated by a homogeneous time resolved fluorescence (HTRF) method.

Aggregation, FROUNT, Oligomer

[Results and discussion]

The scheme for the suppression of aggregation is shown in Figure 1. We analyzed ^{1}H-^{15}N HSQC spectra at different protein concentrations and selected the residues that showed concentration-dependent signal changes. Line-broadening of NMR signals was observed upon the addition of 50 mM NaCl, suggesting that FNT-C forms an aggregate due to hydrophobic interactions. NMR titration experiments using a hydrophobic compound, which we identified, revealed the aggregation sites of FNT-C. The residues forming the aggregation sites were replaced with charged amino acid residues. The FNT-C mutants gave high intensity and well dispersed NMR signals in the ^{1}H-^{15}N HSQC spectra (Figure 2). The analyses of DLS and gel-filtration chromatography showed that an FNT-C mutant is stably monomeric. The HTRF experiments showed that the FNT-C mutants retained the CCR2-binding activity.

[Perspectives]

We will determinate the FNT-C structure, and identify binding surfaces for several kinds of binding partners, using the obtained mutant.

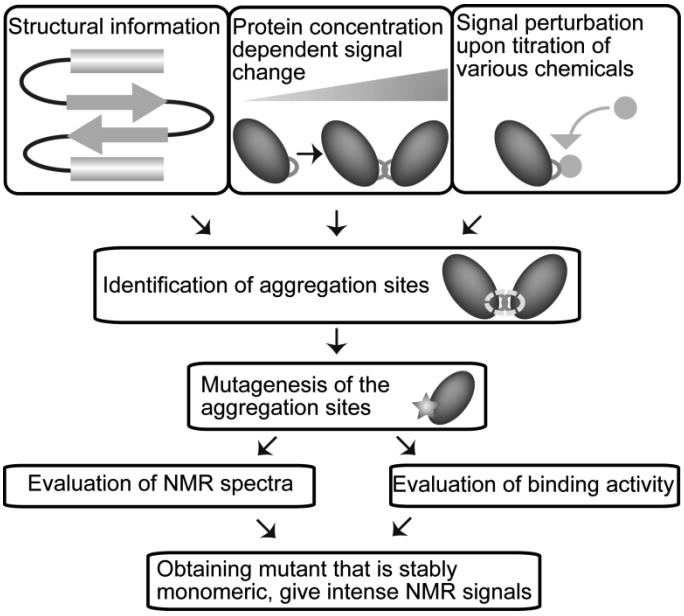

Fig.1. Strategy for suppression of aggregation.

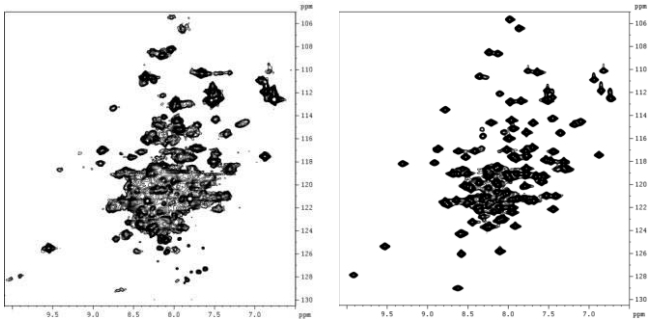

Fig.2. Comparison of the ^{1}H-^{15}N HSQC spectra of wild type FNT-C (left) and FNT-C mutant (right).

[References]

[1] Bagby, S. *et al.*, *J. Biomol. NMR*, **339**, 20–41 (1997)
[2] Sun, Z. *et al.*, *EMBO J.*, **18**, 2941–2949 (1999)
[3] Terashima, Y. *et al.*, *Nature Immunol.*, **6**, 827–835 (2005)
[4] Marsh, J. *et al.*, *Protein Sci.*, **15**, 2795–2804 (2006)

P-015 Development of metabolic isotope-labeling techniques for NMR spectroscopic analyses of high-mannose-type oligosaccharides

Yukiko Kamiya[1], Sayoko Yamamoto[1,2], Yasunori Chiba[3], Yoshifumi Jigami[3], and Koichi Kato[1,2]

[1] Institute for molecular science and Okazaki Institute for Integrative Bioscience National Institutes of Natural Sciences
[2] Graduate School of Pharmaceutical Sciences, Nagoya City University,
[3] Research Center for Medical Glycoscience, National Institute of Advanced Industrial Science and Technology

Accumulating evidence indicates that a variety of intracellular lectins recognize partially trimmed intermediates of the high-mannose-type oligosaccharides and thereby determined the fates of their carrier proteins, i.e. folding, translocation, and degradation [1, 2]. However, the molecular mechanisms of this quality control system remain to be fully elucidated. For better understanding the structural bases of these mechanisms, it is essential to obtain information on structure and dynamics of the oligosaccharide in free as well as lectin-bound states. Although NMR spectroscopy has great potential to provide us with structural information on oligosaccharides in solution at atomic resolution, carbohydrate NMR analyses are frequently hampered by the low sensitivity, the severe spectral overlapping, and the insufficiency of conformational restraints. Recently emerging higher magnetic fields (beyond 900 MHz) provide an increase in sensitivity and chemical shift dispersion along with improved relaxation properties. Applicability of NMR approach to carbohydrate conformational analyses will be strengthened by combining it with stable isotope labeling of the oligosaccharides. However, methodology of stable isotope labeling of sugar chains has been largely unexplored, especially for larger, branched oligosaccharides. Here, we report a novel technique for overexpression of a homogeneous oligosaccharide with ^{13}C labeling by using genetically engineered yeast strains.

To prepare a homogeneous high-mannose-type oligosaccharide in large quantities, we used a mutant strain of *Saccharomyces cerevisiae* with deletions of three genes encoding the enzymes in the processing pathway of *N*-glycans, i.e., Och1p, Mnn1p, and Mnn4p, for enrichment of $Man_8GlcNAc_2$ (M8). This mutated yeast cells were grown in minimum medium containing 0.5% D-[UL-$^{13}C_6$] glucose. The *N*-glycans were released by hydrazinolysis from the glycoproteins produced by the yeast mutant and subsequently re-*N*-acetylated and then fluorescence-labeled with 2-aminopyridine (PA). The PA-derivative was isolated by HPLC and subjected to 920.7 MHz NMR measurements.

The ^{1}H-^{13}C HSQC spectra of M8-PA labeled by using [UL-$^{13}C_6$] glucose as a metabolic precursor exhibited the peaks originating from all the C-H groups (Figure 1A). We further attempted to obtain M8 labeled with ^{13}C at selected carbon positions by culturing the yeast cells using appropriate metabolic precursors. Figure 1B shows ^{1}H–^{13}C HSQC spectra of the pyridylamino derivatives of M8 produced in the engineered yeast cells grown in minimum medium that contains glucose labeled with ^{13}C at carbon position C1, C2, C3, C4, C5, or C6. The spectral data demonstrate that selective ^{13}C enrichment can be achieved at specific positions of each sugar

residue, accelerating peak classification in spectral assignments of the oligosaccharide.

Thus, we successfully developed the metabolic ^{13}C-labeling method, providing the technical basis for NMR analyses of structures, dynamics and interactions of larger, branched oligosaccharides such as high-mannose-type oligosaccharides.

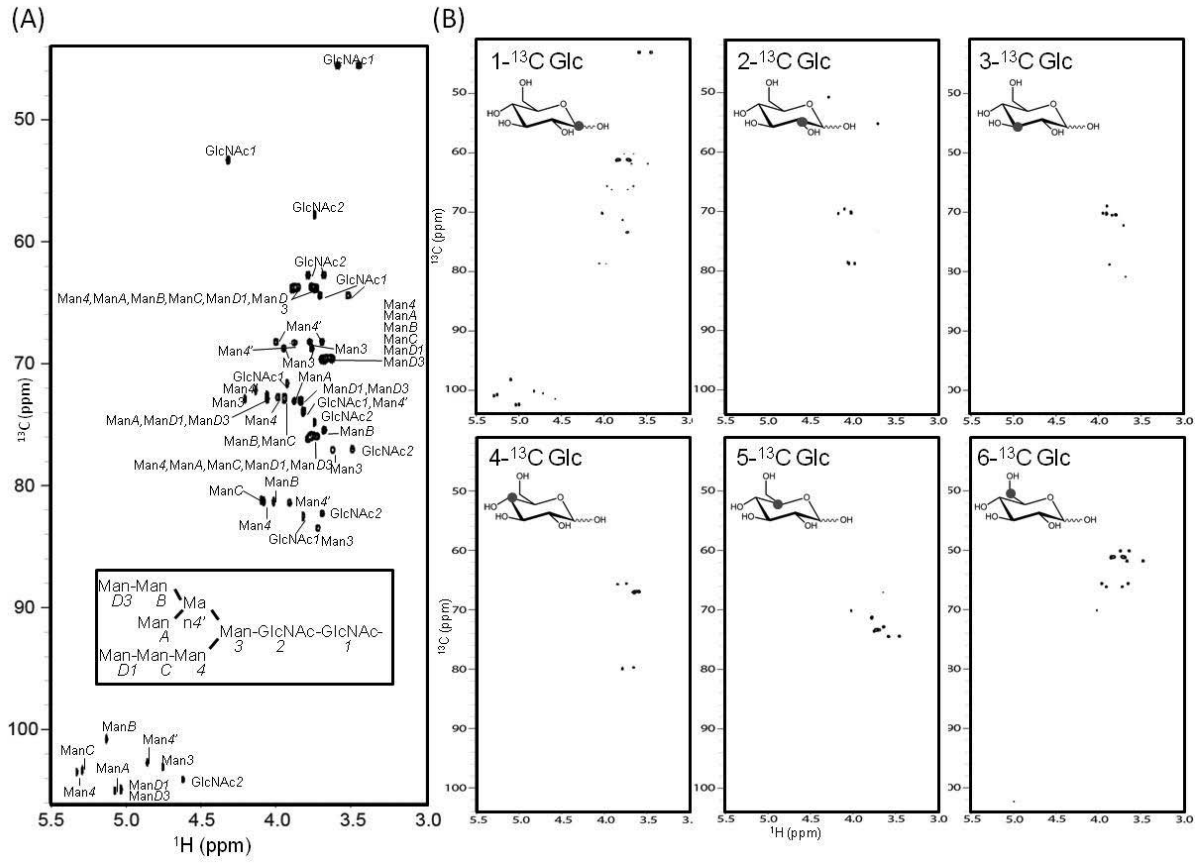

Figure 1
^{1}H–^{13}C HSQC spectra of the pyridylamino derivative of M8, metabolically ^{13}C-labeled using (A) D-[UL-$^{13}C_6$]glucose and (B) D-[1-^{13}C]glucose, D-[2-^{13}C]glucose, D-[3-^{13}C]glucose, D-[4-^{13}C]glucose, D-[5-^{13}C]glucose, or D-[6-^{13}C]glucose. The carbohydrate sequence of M8 is shown in A. In B, the ^{13}C-labeled positions in the glucose isotopomers used as metabolic precursors are shown with *gray circles*.

[References]
1. Y. Kamiya, D. Kamiya, R. Urade, T. Suzuki, and K. Kato, *Glycobiology Research Trends*, **27**, G. Powell and O. McCabe Eds, NOVA Science Publishers, New York, (2009)
2. K. Kato, and Y. Kamiya, *Glycobiology*, (2007) **17**, 1031-1044
3. Y. Kamiya, S. Yamamoto, Y. Chiba, Y. Jigami, and K. Koichi, *J. Biomol. NMR* (2011) **50**, 97-401

Oligosaccharide, ^{13}C labeling, Engineered yeast

P-016 NMR structure and dynamics of the C-terminal domain of an R-type lectin from earthworm in complex with lactose

Hikaru Hemmi[1], Atsushi Kuno[2], Sachiko Unno[2] and Jun Hirabayashi[2]
[1]NARO Food Research Institute, National Agricultural and Food Research Organization (NARO) and
[2]Research Center for Medical Glycoscience, National Institute of Advanced Industrial Science and Technology (AIST).

ABSTRACT

A novel 29-kDa lectin (EW29) isolated from the earthworm *Lumbricus terrestris* consists of two homologous domains (14,500 Da) showing 27% identity with each other [1]. Recently, the crystal structure of the complex between the C-terminal domain of EW29 (EW29Ch) and sugar was reported, indicating that the protein has two sugar-binding sites in subdomains α and γ [2]. The physiological function of EW29, however, remains unknown. In our recent paper [3], NMR titration experiments showed that the α sugar-binding site had a slow exchange regime on the chemical shift timescale for lactose (Kd = 0.01-0.07mM), whereas that the γ sugar-binding site had a fast exchange regime for lactose (Kd = 2.66mM). Thus, the α sugar-binding site has a much tighter sugar-binding mode than the γ sugar-binding site. Although the crystal structure of the complex between EW29Ch and lactose was reported, it is still unclear why the α sugar-binding site binds to lactose more strongly because in the crystal structure of the EW29Ch-lactose complex the interactions between the α sugar-binding site of EW29Ch and lactose are very similar with those between the γ sugar-binding site and lactose.

In this study, we have determined the high-resolution NMR structure of the α sugar-binding site of EW29Ch in complex with lactose ([lactose]/[EW29Ch] = 8) using multinuclear, multidimensional NMR spectroscopy. In addition to 3D ^{15}N-edited NOESY and ^{13}C-edited NOESY spectra of EW29Ch in the lactose-binding state using the mixture of [^{13}C, ^{15}N]-labeled EW29Ch and non-label lactose, we collected 3D ^{13}C-edited NOESY spectrum of lactose in the protein-binding state using the mixture of non-label EW29Ch and ^{13}C-labeled lactose in order to assign the intermolecular NOEs between EW29Ch and lactose accurately. In the [^{13}C,^{1}H]-HSQC spectra of ^{13}C-labeled lactose upon the addition of non-label EW29Ch, changes largely in chemical shift were observed for some NMR signals of the lactose. To assign the NMR signals of the lactose largely changed we collected NMR data using uniform or selective ^{13}C-labeled lactose and a series of selective ^{13}C-labeled galactose because it is very hard to assign the NMR signals using the conventional NMR methods. The results from changes in chemical shift of the lactose upon addition of EW29Ch indicated that EW29Ch interacted with the galactose residue of lactose molecule. Thus, these results confirmed our previous data from the STD-NMR experiments of lactose with EW29Ch [3]. Next, comparing of NMR structure of EW29Ch bound to lactose determined in this study with that of EW29Ch in the sugar-free state, the slight differences were

Lectin, Sugar, Interaction

observed at some loop regions and some residues related with sugar-binding. Further, we compared the sugar-binding mode of the α sugar-binding site of EW29Ch in NMR structure of EW29Ch-lactose complex with that of the crystal structure of the complex between EW29Ch and lactose. The results showed that the interactions between EW29Ch and lactose in the NMR structure were similar to those in the crystal structure of EW29Ch-lactose complex.

We also performed the NMR relaxation experiments (^{15}N T_1, ^{15}N T_2, and ^{15}N{^{1}H}-NOE) for the backbone of EW29Ch in the sugar-free state or in the complex with lactose. The results showed that the differences of the relaxation data between the two states were particularly observed for the α sugar-binding site even though the sugar-binding mode of the α sugar-binding site in the NMR structure of EW29Ch in complex with lactose is similar with that in the crystal structure of the EW29Ch-lactose complex. We will discuss the relationship between the motions of the backbone of EW29Ch and the sugar binding.

References

1. Hirabayashi, J., Dutta, S. K., and Kasai, K. (1998) J. Biol. Chem. 273, 14450-14460.
2. Suzuki, R., Kuno, A., Hasegawa, T., Hirabayashi, J., Kasai, K., Momma, M., and Fujimoto, Z. (2009) Acta Crystallogr D 65, 49-57.
3. Hemmi, H., Kuno, A., Ito, S., Suzuki, R., Hasegawa, T., and Hirabayashi, J. (2009) FEBS J. 276, 2095-2105.

P-017 A telomeric repeat-binding factor TRF2 binds to a parallel G quadruplex structure formed by single telomeric DNA via its Myb domain

Yuuka Hirao, Shin Morita, Kazuki Oinishi, Hideaki Shimojo, Shingo Hanaoka, Hideyasu Okamura, Tadateru Nishikawa and Yoshifumi Nishimura
Division of Supramolecular Biology, Graduate School of Nanobioscience, Yokohama City University

ABSTRACT

Human telomeres consist of double stranded TTAGGG repeats followed by the single stranded repeats at 3' end and shelterin proteins, including hTRF1 and hTRF2. The single stranded tail in telomeres could form G quadruplex (G4) structure. We show that the Myb domain of hTRF2 binds to a parallel G4 structure formed by the single stranded TTAGGGTTAGGG sequence by NMR. We also demonstrate by mutation and NMR experiments that the second helix in the hTRF2 Myb domain is responsible for the interaction with the parallel G4 structure by a different manner from the dsDNA binding of hTRF2 Myb domain.

INTRODUCTION

Telomeres are protein-DNA complexes that distinguish natural chromosome ends from damaged DNA. Mammalian telomeric DNA is composed of long tandem arrays of double stranded DNA (dsDNA) with a repetitive TTAGGG sequence followed by a short single stranded DNA (ssDNA) sequence at the 3' ends. The TTAGGG repeats associate with a protein complex composed of six proteins called Shelterin consisting of TRF1, TRF2, Rap1, TPP1, TIN2 and Pot1. TRF1 and TRF2 are mammalian telomeric dsDNA-binding factors. They contain a similar dsDNA binding domain (DBD) in their C-termini and a central conserved TRF-homology (TRFH) domain. At the N terminus, TRF1 has an acidic domain, while TRF2 has a basic domain. TRF1 and TRF2 can bind to dsDNA. The structures of the complexes of telomeric dsDNA with the Myb domains of hTRF1 and hTRF2 are very similar to each other, consisting of a three α-helical bundle.

The ssDNA tails of telomeres have the potential to form a G4 structure stabilized by four guanine residues in a plane connected by Hoogsteen type hydrogen bonds. Several G4 structures have been found with the differences dependent upon ssDNA sequence, ssDNA chain length and monovalent counter cation such as sodium and potassium ions.

Here we found that $(TTAGGG)_2$ in potassium ion solutions could form a parallel form G4 structure. Also we have examined the binding activities of hTRF1 and hTRF2 DBD to several characteristic G4 structures including a basket type formed by $d(AG_3(TTAGGG)_3)$, a (3+1) type G4 structure of $TTGGG(TTAGGG)_3A$ and a G4 structure formed by $(TTAGGG)_2$ and we reveal a specific interaction of hTRF2 Myb DNA-binding domain with the parallel G4 structure by NMR.

MATERIALS AND METHODS

hTRF1 DBD, hTRF2 DBD and seven mutants of hTRF2 DBD (Q463R, A471S, A472K, S474L,

Keywords: telomere, G-quadruplex, TRF2

K475L, N476H and 6M) were purified.

The oligonucleotide fragments, 5'-$(TTAGGG)_2$-3' (tr12), 5'-TAGGGTTAGGGT-3' (tr12x), 5'-AGGG$(TTAGGG)_3$-3' (tr22), 5'-TTGGG$(TTAGGG)_3$A-3' (tr24) and isotope-labeled tr12 with ^{15}N and ^{13}C were dissolved in sodium phosphate buffer to form Na type G4 structures and into potassium phosphate buffer to form K type G4 structures, and then annealed.

We measured two kinds of NMR titration experiments: 1D ^{1}H NMR spectra of DNA by adding protein samples and 2D ^{1}H-^{15}N HSQC spectra of each protein sample by adding DNA.

RESULTS AND DISCUSSION

CD and 1D ^{1}H NMR spectra of DNA suggested that tr12-K could form a parallel G4 structure and tr24-K and tr22-Na had the same structures that reported before. However, imino proton signals of tr12x-K, tr22-K and tr12-Na could not be well resolved which is indicative that they have mixed G4 structures. (Fig.1)

From monitoring the imino proton signal for each of tr12-K, tr22-Na and tr24-K after adding hTRF2 DBD, the signals of tr12-K shift significantly to lower fields by addition of hTRF2 DBD, while significant shifts of the imino proton signals of tr22-Na and tr24-K could not be detected. The chemical shifts for the interaction between hTRF2 DBD and tr12-K suggest a specific interaction, while the shifts for tr22-Na and tr24-K suggest non specific interactions.

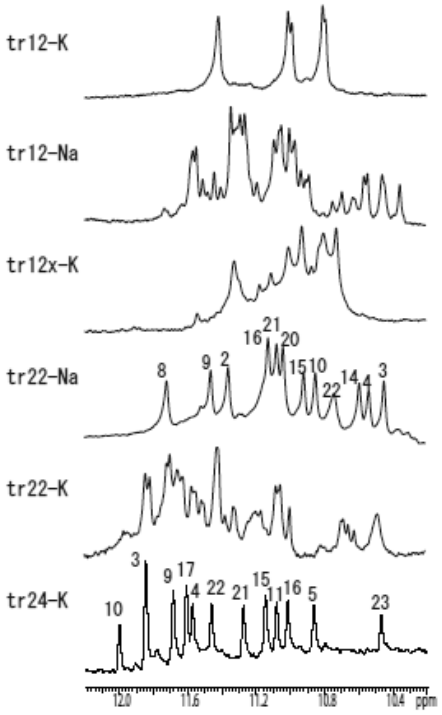

Fig.1 The imino proton signals of several G4 structures.

Next we examined ^{1}H-^{15}N HSQC spectral changes of hTRF2 DBD after addition of each of the G4 structures. The signals of V462 to N476 in hTRF2 DBD changed significantly after adding tr12-K.(Fig.2) These amino acids are located in the end of helix 1, the turn between helix 1 and 2 and most of helix 2. It is therefore clear that hTRF2 DBD has the specific ability to bind the tr12-K G4 structure (which is a parallel G4 structure) in a different manner to the dsDNA binding mechanism of hTRF2 DBD. This means that hTRF2 DBD is considered to have dual faces; one face is involved in the interaction with dsDNA and the other face is involved in the interaction with a parallel G4 structure formed by single stranded DNA.

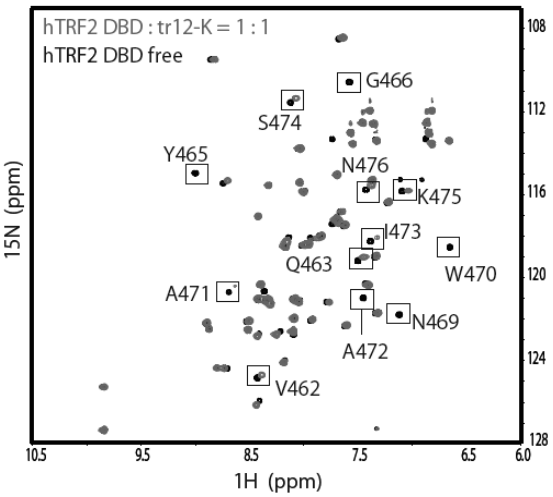

Fig.2 ^{1}H-^{15}N HSQC spectral changes in hTRF2 DBD in the presence of tr12-K

In order to determine the amino acids of hTRF2 DBD responsible for the interaction with tr12-K G4, we examined the binding activity of hTRF2 mutants to tr12-K G4 structure. As a result, it is apparent that the A471S, A472K, S474L, K475L and 6M mutants have weaker binding ability to tr12-K G4 structure compared to the wild type. This means that these 4 amino acids are important for the interaction with tr12-K.

P-018 Aromatic Side-Chain Dynamics in FKBP Proteins Characterized by the SAIL Method for Free and Ligand-Bound States

Chun-Jiun Yang[1], Mitsuhiro Takeda[2], JunGoo Jee[1], Akira Mei Ono[3], Tsutomu Terauchi[3], and Masatsune Kainosho[1,2]

[1]Graduate School of Science and Engineering, Tokyo Metropolitan University, [2] Graduate School of Science, Nagoya University, and [3] SAIL Technologies

ABSTRACT

Stereo-array isotope labeled (SAIL) amino acids with optimized labeling patterns facilitate accurate structure determinations of larger proteins, and also offer various new methods for studying protein dynamics. Site-specific ^{2}H- and ^{13}C-labeling at alternative positions simplifies the NMR signals of aromatic rings, and also affords unprecedented opportunities to study ring-flipping dynamics in detail. We have applied the SAIL method to FKBP12 and FKBP12.6, using various types of SAIL-Tyr. In this presentation, we report the hydrogen exchange rates of the hydroxyl groups and the ring flipping motions of tyrosine residues for these two proteins, in the free and ligand-bound states. Both dynamic characteristics became much slower upon ligand binding. Furthermore, even though the two structurally-related tight binders, FK506 and rapamycin, used in this study associate with FKBP12 in almost identical modes, the tyrosine ring dynamics revealed distinct behaviors for these two complexes.

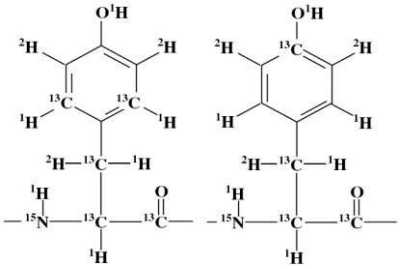

Fig. 1 δ-SAIL Tyr (left) and ζ-SAIL Tyr (right).

An intimate relationship exists between the dynamics and the biological functions of proteins. Although aromatic rings usually reside at protein-protein and protein-ligand binding interfaces, knowledge of the side-chain motions of these bulky residues has been quite limited, until now. NMR is the most suitable tool to provide site-specific information about dynamic processes over a large time-scale. However, the minimal chemical shift dispersion of aromatic ring resonances hampers unambiguous assignment and accurate data analysis. Due to these problems, it has been difficult to study the aromatic side-chain dynamics with conventional, uniformly ^{13}C labeled proteins. The SAIL (Stereo-Array Isotope Labeling) method using optimized labeling patterns affords excellent probes to monitor protein motions. For example, in the aromatic amino acids, the site-specific ^{2}H- and ^{13}C-labeling at alternative positions (Fig. 1) not only simplifies the NMR signals, but also gives superb spectral qualities, by removing tight spin couplings. Here, we utilized the strength of the SAIL method to simultaneously characterize the hydrogen exchange rates of hydroxyl groups and the ring flipping motions of tyrosine residues upon ligand binding.

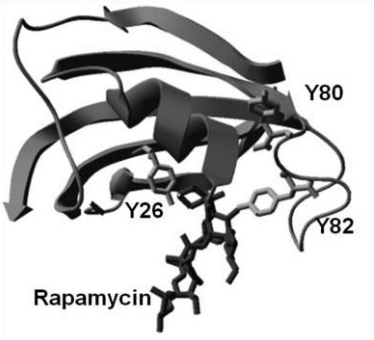

Fig. 2 Crystal structure of FKBP12- rapamycin complex. Tyrosine residues were labeled and emphasized. Backbone region of residues 46-55 was hidden for clarity.

SAIL, Aromatic Side-Chain Dynamics, Protein-Ligand Interaction

FKBP12 (Fig. 2) and its closely related FKBP12.6 isoform (sharing 83% sequence identity), labeled with various types of SAIL-Tyr (Fig. 1), were prepared. Both proteins exhibit peptidyl-prolyl *cis-trans* isomerase activities and bind to two structurally-related ligands, FK506 and rapamycin, with comparable affinities. Due to the two-bond deuterium isotope effects, the chemical shifts of Tyr $^{13}C^{\zeta}$ resonances connected with an OH or OD group are different. Up-field shifts will be observed in the deuterium-substituted species. Therefore, in a solution of 1:1 H_2O and D_2O, a split signal of $^{13}C^{\zeta}$ will be detected in ^{13}C spectra, if the exchange rate of the hydroxyl hydrogen to the surrounding waters is sufficiently slow. While the H/D exchange rates of hydroxyl protons were fast in the free form of FKBP12 or FKBP12.6, as revealed by singlet $^{13}C^{\zeta}$ signals in the H_2O/D_2O mixture, the $^{13}C^{\zeta}$ peaks of Tyr26 and Tyr82 appeared as doublets in the complex with rapamycin or FK506, implying slow exchange (Fig. 3). Ligand binding caused a considerable reduction in the aromatic ring flipping motion. Separated signals from equivalent positions, namely δ1 and δ2 ^{1}H-^{13}C or ε1 and ε2 ^{1}H-^{13}C, of Tyr26 were observed when FKBPs associated with FK506; however, only averaged signals showed in the free form (Fig. 4). Interesting, even though rapamycin binds to FKBP12 in an almost identical mode, as compared to FK506, the flipping motion of Tyr26 revealed distinct timescales in these two complexes. Line broadened signals were detected at ambient temperature, suggesting that the flipping motion of Tyr26 in the rapamycin complex was somewhat faster than in the FK506 complex. We will further quantify the flipping and hydroxyl proton exchange rate constants in the ligand-bound states with rapamycin and FK506. The relationship between the aromatic side-chains motions and the ligand binding will also be discussed.

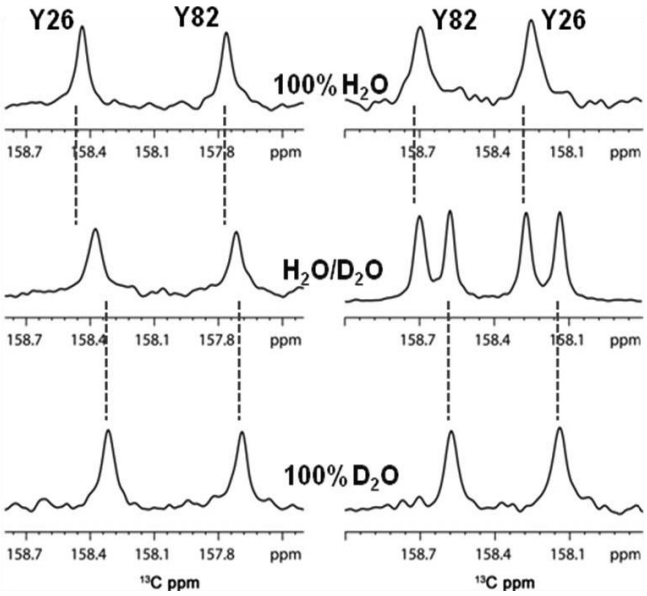

Fig. 3 1D ^{13}C spectra of ζ-SAIL-Tyr selectively labeled FKBP12.6 in free (left) and rapamycin bound (right) state in 100% H_2O (top), H_2O/D_2O mixture (middle), and 100% D_2O (bottom) at 30 degree.

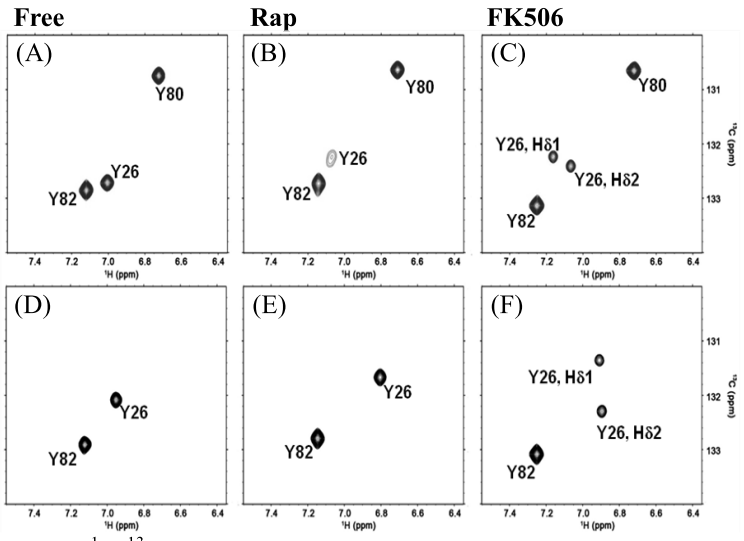

Fig. 4 ^{1}H-^{13}C HSQC spectra of δ-SAIL Tyr selectively labeled FKBP12 (A-C) and FKBP12.6 (D-F) in free and ligand-bound states as indicated on top margin at 30 degree.

REFERENCES

1. Kainosho, M. et al. (2006) *Nature,* 440, 52-57.
2. Takeda, M., Ono, A. M., Terauchi, T. & Kainosho, M. (2009) *J Biomol NMR,* 46, 45-49.
3. Takeda, M., Jee, J., Ono, A. M., Terauchi, T. & Kainosho, M. (2009) *J Am Chem Soc,* 131, 18556-18562.

P-019 Structural characterization of carbon monoxide adduct of a complex between heme and a parallel G-quadruplex DNA

Hulin Tai,[1] Kaori Saito,[1] Masashi Fukaya,[1] Tomokazu Shibata,[1]
Saburo Neya,[2] and Yasuhiko Yamamoto[1]
[1] Department of Chemistry, University of Tsukuba
[2] Graduate School of Pharmaceutical Sciences, Chiba University

ABSTRACT The structure of a carbon monoxide (CO) adduct of a complex between heme and a parallel G-quadruplex DNA has been characterized. The study revealed that the heme binds to the 3'-terminal G-quartet, and the π-π stacking interaction between the pseudo-C_2 symmetric heme and the C_4 symmetric G-quartet in the complex resulted in the formation of two isomers (with a ratio of ~1:1) possessing heme orientations differing by 180° rotation about the pseudo-C_2 axis, with respect to the DNA. Exogenous CO is coordinated to heme Fe on the side of the heme opposite the G-quartet, and the nature of the Fe-CO bond in the complex is similar to those in hemoproteins.

INTRODUCTION The G-quartet is formed from four guanine bases that are cyclically associated through Hoogsteen hydrogen-bonding (Fig. 1A). The size and planarity of the G-quartet are well-suited for interaction with heme (Fe-protoporphyrin complex (Fig. 1B)) through π-π stacking. Characterization of the molecular recognition between heme and the G-quartet is expected to provide knowledge for not only designing a stable complex between heme and DNA, but also for tuning of the heme reactivity in the scaffold of the DNA structure. Previously, we demonstrated the formation of a stable complex between heme(Fe^{3+}) and parallel G-quadruplex DNA assembled from a single repeat sequence of the human telomere, d(TTAGGG),[1] and that carbon monoxide (CO) can bind to the heme(Fe^{2+})-DNA complex.[2] In this study, we have investigated the molecular recognition between heme(Fe^{2+}) and the DNA in a CO adduct of the complex.

RESULTS AND DISCUSSION

^{13}C NMR spectrum of the ^{13}CO adduct of the heme-DNA complex. The ^{13}C NMR spectrum of the ^{13}CO adduct of the heme-DNA complex is compared with that of the ^{13}CO form of myoglobin (Mb) in Fig. 2. In the spectrum of Mb, two signals due to heme Fe^{2+}-bound and free ^{13}CO were observed at 207.03 and 184.06 ppm, respectively (Fig. 2A).[3] Similarly, two separate signals were observed at 206.81 and 184.11 ppm, in the complex (Fig. 2B). Based on comparison of the two spectra, the signals at 206.81 and 184.11 ppm can be unambiguously assigned to ^{13}CO bound to heme Fe^{2+} of the complex and free ^{13}CO, respectively. The similarity in the shift of the ^{13}CO signal between the heme-DNA complex and Mb indicated that nature of the Fe^{2+}-^{13}CO bond in the complex is similar.

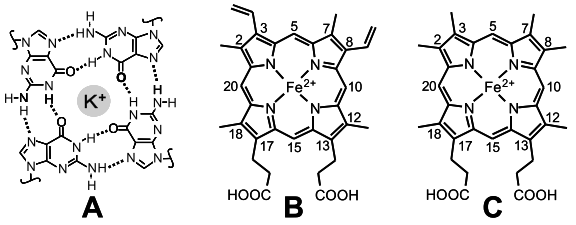

Fig. 1. Molecular structures of G-quartet (A), heme (B), and Fe^{2+}-3,8-dimethyldeuteroporphyrin complex (DMheme) (C).

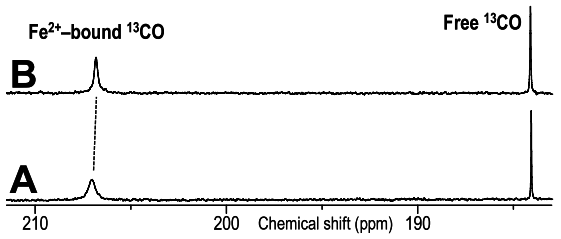

Fig. 2. 125 MHz ^{13}C NMR spectra of ^{13}CO form of Mb (A) and ^{13}CO adduct of the heme-DNA complex (B) in 90% H_2O/10% ^2H_2O, 300 mM KCl, pH7.0, at 25°C.

^{1}H NMR spectra of the CO adduct of heme-DNA complex. ^{1}H NMR spectra of $(d(TTAGGG))_4$ and the CO adduct of heme-DNA complex are compared with each other in Fig. 3. The $(d(TTAGGG))_4$ was manifested in the observation of three exchangeable proton signals, due to guanine imino NH protons, in the chemical shift region characteristic of G-quartets (Fig.3A and A'). As was reported previously,[4] $(d(TTAGGG))_4$ forms a dimer through end-to-end stacking of the 3'-terminal G-quartets in the presence of high [K+] (Fig. 3A). In the spectrum of the DNA in the

Keywords: G-quadruplex DNA, Heme, NMR

presence of [K^+] = 50 mM, guanine imino NH proton signals arising from both the monomer and dimer of the DNA were observed (Fig. 3A'').[4] In the spectrum of the CO adduct of the heme-DNA complex, the guanine imino NH proton signals could be readily identified through analysis of the effects of ^2H_2O content in the sample solutions on the spectra (Fig. 3B and b). The guanine imino NH protons in CO adduct of the heme-DNA complex are ranked as G4 < G5 < G6, in order of increasing heme ring current-induced shift change ($\Delta\delta_{hisc}$), *i.e.*, values of -0.37, -0.87, and -2.54 (or -2.49) ppm, relative to the corresponding signals of the $(d(TTAGGG))_4$ monomer, were observed for the G4, G5, and the G6 proton signals, respectively. In addition, intermolecular NOE connectivities between heme vinyl protons and G6 sugar H1' and base H8 protons signals also observed (data not shown). Furthermore, analysis of the intensities of the heme *meso* and DNA A3-H8 protons indicated a stoichiometric ratio of 1:1 for heme:DNA in the complex. These results not only indicated that heme stacks onto G6 G-quartet (Fig. 3D), but also suggested that the heme located at ~0.40 nm from the G6 G-quartet reasonably satisfies the $\Delta\delta_{hisc}$ values for the guanine imino NH proton signals.[5] Considering that the Fe-CO fragment is ~0.43 nm in length, it is unlikely that the axial CO is coordinated to the Fe atom on the G-quartet side of the heme (Fig. 3D).

Interestingly, the G6 imino NH proton signal of the complex split into two peaks with an intensity ratio of ~1:1 (Fig. 3B). Similarly, two sets of signals, in a ratio of ~1:1, were also observed for most of the heme protons (data not shown). In order to determine the reason for the appearance of the two sets of signals for these protons, the spectrum of the CO adduct of the complex between C_2 symmetric DMheme (Fig. 1C) and $(d(TTAGGG))_4$ was analyzed (Fig. 3C). The obtained signal assignments indicated that, only a single set of signals was observed for the DMheme-DNA complex, as reflected in the absence of the splitting of the G6 imino NH proton signal (Fig. 3C). These results demonstrated that the ~1:1 splitting of some ^1H NMR signals of the heme-DNA complex is due to the pseudo-C_2 symmetry of the heme molecular structure (Fig. 3E).

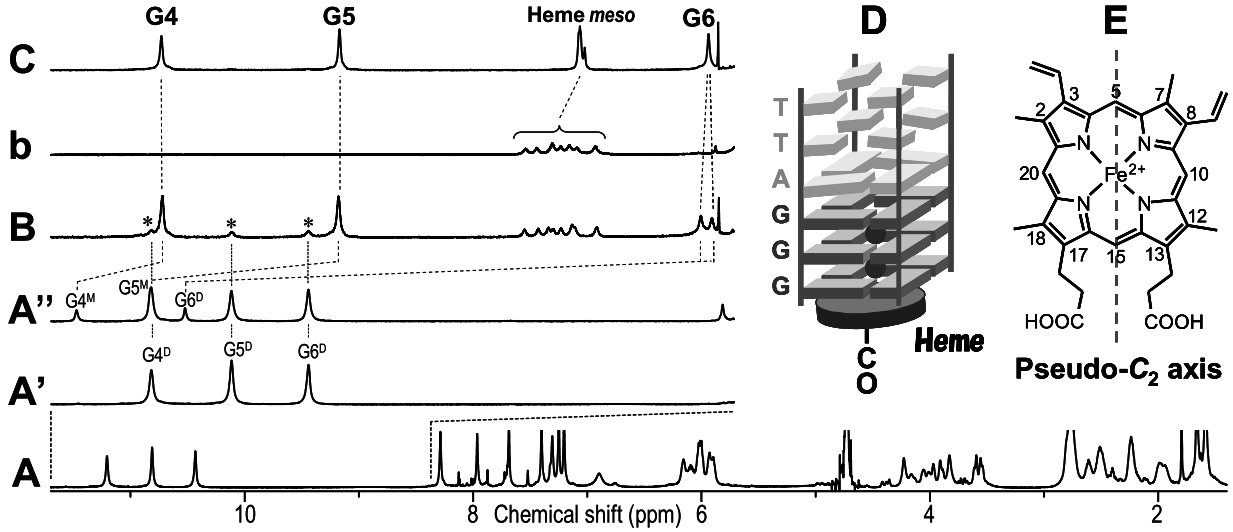

Fig. 3. 600 MHz ^1H NMR spectrum of $(d(TTAGGG)_4)$ (DNA) in 90% H_2O/10% ^2H_2O (A), and downfield portions, 8.33 – 11.70 ppm, of the spectra of DNA in 90% H_2O/10% ^2H_2O (A' and A''), CO adduct of heme-DNA complex in 90% H_2O/10% ^2H_2O (B) and in 100% ^2H_2O (b), and CO adduct of DMheme-DNA complex in 90% H_2O/10% ^2H_2O (C). Sample A'' was prepared in 50 mM KCl, and the others in 300 mM KCl. Gn^D and Gn^M, where n = 4, 5, or 6, represent the dimer and monomer of the DNA, respectively. Schematic representation of the structure of CO adduct of the heme-DNA complex (D) and pseudo-C_2 symmetry axis of heme (E)

CONCLUSION The study revealed that, heme(Fe^{2+}) stacks onto the G6 G-quartet of the DNA, and that the heme(Fe^{2+}) plane is located at ~0.40 nm from the G6 G-quartet one, with the two orientations differing by 180° rotation about the 5-H-15-H axis, with respect to the DNA. These findings provide novel insights as to the design of heme-deoxyribozymes and –ribozymes.

REFFERRENCES: [1] T. Mikuma *et al.*, ***Chem. Commun.***, **14**, 1708-1709 (2003). [2] K. Saito *et al.*, ***Nucleic Acids Symp. Ser.***, **53**, 241-242 (2009). [3] K. D. Park *et al.*, ***Biochemistry***, **30**, 2333-2347 (1991). [4] Y. Kato *et al.*, ***J. Am. Chem. Soc.***, **127**, 9980-9981 (2005). [5] R. J. Abraham *et al.*, ***Magn. Reson. Chem.***, **26**, 803-812 (1988).

P-020
Y

NMR structure of the HP1-α chromodomain phosphorylated at N-terminal serine residues

Ayumi Kawaguchi[1], Hideaki Shimojo[1], Kyoko Hamada[2], Jun-ichi Nakayama[2] and Yoshifumi Nishimura[1]
[1] Department of Supermolecular Biology, Graduate School of Nanobioscience, Yokohama City University, Kanagawa, Japan
[2] Laboratory for Chromatin Dynamics, Center for Developmental Biology, RIKEN, Kobe, Japan

ABSTRACT

Recently we revealed that HP1α was multiply phosphorylated at N-terminal serine residues (S11-14) in human and mouse. The phosphorylation appeard to facilitate the initial binding of HP1α to methyllysine at residue 9 of histone H3 tail (H3K9me). Unphosphorylatable mutant HP1α exhibits severe heterochromatin localization defects in vivo, and its prolonged expression led to increased chromosomal instability. This suggests that HP1α's N-terminal phosphorylation is essential for heterochromatin formation. Here, we determine the NMR structure of the phosphorylated HP1α chromodomain to reveal its interaction mode with the metylated histone tail.

INTRODUCTION

In eukaryotic cells, DNA is stored stably in a highly ordered structure, chromatin. Its fundamental repeating structural unit is a nucleosome core, which is comprised of a histone octamer and 147bp DNA. Heterochromatin protein 1 (HP1) is a conserved chromosomal protein and plays important roles in chromatin packaging. All HP1 homologues contain two functionally distinct globular domains, the N-terminal chromodomain and the C-terminal chromoshadow domain. The chromodomain of HP1 recognizes H3K9me, causing epigenetic silencing. The methyl ammonium group is captured by three aromatic side chains by cation-π and van der-Waals interactions.

EXPERIMENTAL

For obtaining the phosphorylated HP1α chromodomain (phosHP1αCD), recombinant 6×His-tagged HP1αCD and casein kinase-2(CK2) were co-expressed in *E coli* BL21(DE3). The cells were grown in M9 minimal medium containing [^{15}N] ammonium chloride and [^{13}C] glucose. The cells were lysed by sonication and centrifuged. The supernatant was applied through nickel-nitilotriacetic acid (NTA) chromatography. The sample was digested with Thrombin protease to remove His-tag and again loaded onto the Ni-NTA agarose column. The phosHP1αCD was further purified by gel filtration chromatography.

The concentration of proteins for NMR experiments was about 0.5 mM in 20mM KPB (pH 6.8), 10mM NaCl,5mM DTT dissolved in either 90% H_2O/10% D_2O or 99.9% D_2O. NMR experiments were carried out at 25°C on Bruker AVANCE-500,600 or 700 equipped with cryoprobe. The structure of the phosHP1αCD was determined by hetero nuclear multidimensional NMR experiments. All NMR spectra were processed using the program NMRPipe and analyzed using program Olivia. The structure was calculated by program CYANA.

HP1, chromatin remodeling, chromodomain

RESULTS & DISCUSSIONS

We examined the binding abilities of the phosHP1αCD to the H3K9me peptide using NMR. By comparison of the $^{1}H,^{15}N$-HSQC spectrum of the phosHP1αCD free with that of its H3K9me peptide complex, we found significant chemical shift changes for some residues that formed the “aromatic cage” and neighboring residues

The phosHP1αCD free structure is essentially same to canonical chromodomain fold despite serine phosphorylation. Especially, amino acids, Y20,W41,F44, which formed a distinct aromatic cage were converged well in NMR structtures.

The serine phosphorylation doesn’t seem to change the tertiary structure but the dynamics of HP1αCD. We are now examining the complex structure of phos-HP1αCD bound to the H3K9me peptide and the interaction mode between the phosHP1αCD and H3K9me.

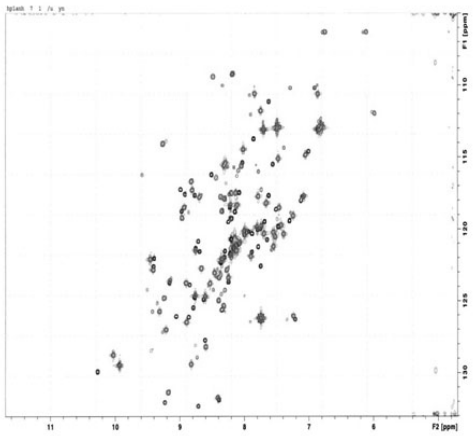

[Fig.1] $^{1}H,^{15}N$-HSQC spectra of phos-HP1αCD free form and its H3K9me peptide complex form.

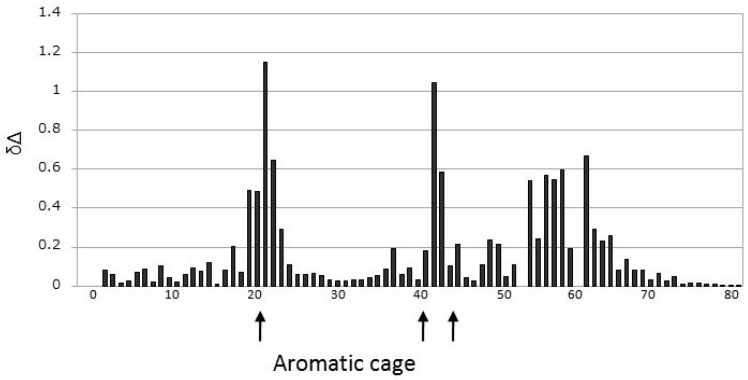

[Fig.2] Chemical shift changes between the phos-HP1αCD free form and H3K9me peptide complex form.

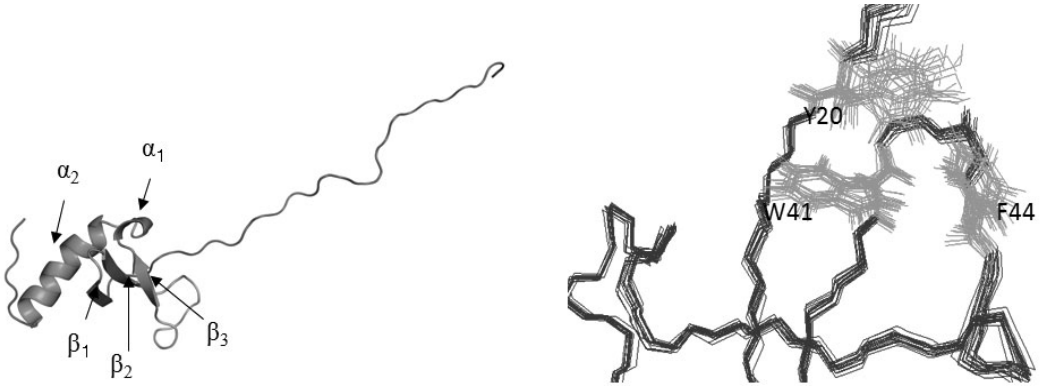

[Fig.3] Solution structure of the phos-HP1αCD (left) schematic ribbon diagram, (right) Best-fit superposition of the final 20 NMR structure of the aromatic cage of phos-HP1αCD

REFERENCES

Hiragami-Hamada,K.,et al.
N-terminal phosphorylation of HP1α promotes its chromatin binding.
Mol. Cell. Biol. 31, 1186-200 (2011)